https://doi.org/10.5194/egusphere-2022-1175
Preprint. Discussion started: 18 November 2022

Role of inheritance during tectonic inversion of a rift system in a thick- to thin-skin transition: Analogue modelling and application to the Pyrenean – Biscay System

Jordi Miró[1], Oriol Ferrer[1], Josep Anton Muñoz[1], Gianreto Manastchal[2]

[1]Institut de Recerca GEOMODELS, Departament de Dinàmica de la Terra i de l'Oceà, Facultat de Ciències de la Terra, Universitat de Barcelona, Barcelona, 08028, Spain
[2]Institut de Physique du Globe de Strasbourg, CNRS-UMR 7516, EOST, Université de Strasbourg, Strasbourg, 67084, France

Correspondence to: Oriol Ferrer (joferrer@ub.edu)

Abstract. The reactivation of former rift systems and passive margins during tectonic inversion and its incorporation into fold-and-thrust belts results into significant structural variability not only between internal to external domains, but also along-strike. The Basque-Cantabrian and Asturian systems are among the best examples to address the role of along-strike changes in rift inheritance since they show a transition from salt to basement inherited structures limited by a transition zone separating thick- from thin-skin structural domains. While both domains have been widely described in the literature, the transfer system separating the two is yet little investigated due to the poor seismic imaging and the lack of large-scale exposures. This contribution aims to address the linkage between basement-controlled (i.e., autochthonous) and salt decoupled (i.e., allochthonous) domains and how deformation is accommodated in the transitional domain in between. An experimental program based on analogue models has been designed inspired by the transition from the thin-skinned Basque – Cantabrian Pyrenees to the east and the thick-skinned Asturian Massif to the west. The experimental results show that oblique structures form in the transitional domain, which position depends on the active structures occurring in both surrounding thick- and thin-skinned domains. Nevertheless, their orientation and evolution are controlled by the underlying decoupling horizon (i.e., salt). The deformation in the thick-skinned domain produces significant topography over a narrow deformation area due to the lack of effective decoupling levels. On the contrary, deformation in the thin-skinned domain is more distributed due to decoupling, resulting in a wider deformation area of less topography. As a result, syn-contractional sedimentation is occurring mainly in the foreland basin in front of the thick-skinned domain, whereas it is observed in the foreland but also in piggy-back basins in the thin-skinned domain.

https://doi.org/10.5194/egusphere-2022-1175
Preprint. Discussion started: 18 November 2022

1 Introduction

The presence of inherited structures and weak horizons at different structural levels are among the most important factors controlling the structural evolution of fold-and-thrust belts (F&TB) (Beaumont et al., 2000; Butler et al., 2006; Amilibia et al., 2008; Miró et al., 2021). In mountain belts, reactivated structures are usually inherited from a preceding rift system or a passive margin. As a result, analysing the inherited extensional structural grain is crucial for the understanding of the structural style and evolution of F&TBs (Carrera et al., 2006, Tugend et al., 2014; Chenin et al., 2017). In addition, the distribution and continuity of weak horizons, such as salt layers, interbedded in the deformed succession also play a significant role in the along-strike variation of the structural style of F&TBs as they act as efficient detachment layers [e.g., Zagros (Molinaro et al., 2005), Andes (Kley et al., 1999), Apennines (Tozer et al., 2002), Pyrenees (Carola et al., 2013)]. Such along-strike variations are expressed by differences in the structural style and final topography, changes in the vergence, the development of salients and reentrants, and the presence of oblique and transverse structures connecting different segments of the orogen (Jaumé and Lillie, 1988; Cotton and Koyi, 2000; Bahroudi and Koyi, 2003; Muñoz et al., 2013; Ghani et al., 2018).

The development of F&TBs reactivating rift systems (i.e., positive inversion sensu Cooper et al., 1989) is widely recognized in thick-skinned structural domains, as the basement is usually involved during the contractional reactivation of inherited extensional faults [e.g., Asturian Massif (Pulgar et al., 1999), Andes (Carrera and Muñoz, 2013; Iaffa et al., 2011a and b)]. On the contrary, the presence of salt layers in the cover succession and pre-contractional salt structures results into a different style of inversion tectonics, dominated by decoupling and squeezing of salt structures [e.g., Pyrenees (Carola et al., 2015; Muñoz et al., 2018), Alps (Granado et al., 2018; Céllini et al., 2020)]. In such circumstances, reactivated subsalt basement-involved faults are laterally shifted, and inversion tectonics can be inferred from differences in the stratigraphic record. The timing of salt deposition related to the main extensional episode (i.e., pre- or syn-rift) as well as its regional distribution within a rifted margin will determine the structural style during the subsequent contractional deformation. For a pre-rift salt, the distribution depends on factors such as the initial salt thickness, the amount and rate of extensional deformation, and the erosion/dissolution in the uplifted footwalls (Rowan, 2014). In the case of syn-rift salt, thickness and facies distribution depend on the geometry of the fault system and the interplay between faults through, sedimentation rate, and environmental depositional conditions (Rowan, 2014).

Scaled analogue models have been widely used to deal with multiple structural problems in rift systems as the structural inheritance in extensional oblique rift systems (e.g. McClay and White, 1995; Amilibia et al., 2005); basement-controlled transfer zones (e.g. Acocella et al., 1999; Wu et al., 2009); the inversion of normal faults with evaporites (e.g. Del Ventisette et al., 2006; Sani et al., 2007; Bonini et al., 2012; Ferrer et al. 2016 and submitted; Roma et al., 2018a and b; Dooley and Hudec, 2020; Wilson et al., submitted) and without evaporites (e.g. McClay, 1989; McClay and Buchanan, 1992; Pinto et al., 2010; Ferrer et al. 2016; Granado et al., 2017); the distribution and impact of salt in thin-skinned extensional settings (e.g. Vendeville and Jackson, 1992; Jackson et al., 1994), and the role of basement faults beneath decoupling horizons (e.g.

https://doi.org/10.5194/egusphere-2022-1175
Preprint. Discussion started: 18 November 2022

Withjack and Callaway, 2000; Dooley et al., 2005, Ferrer et al., 2016 and submitted; Roma et al., 2018a and b; Wilson et al., submitted). On the other hand, there are no experimental programs to address from a three-dimensional point of view the interplay of pre-rift salt and basement structures during formation and inversion of rift systems, regardless it is a relatively common scenario in F&TBs (e.g., Zagros, Pyrenees, Hellenids, among many other contractional systems (Molinaro et al., 2005; Muñoz et al., 2018; Mazzoli et al., 2022)). For this reason, we present a set of 3-D analogue models to investigate how the structural grain inherited from a rifting episode controls the along-strike variation of thick- to thin-skinned deformation in F&TBs. Our experimental program has been inspired by the Asturian Massif and the Basque – Cantabrian Pyrenees case study, where a transition from a non-salt (i.e., thick-skinned) to a salt dominated system (i.e., thin-skinned) respectively occurs. The experimental program presented in this study allows: (1) to understand the along-strike thick- to thin-skinned transition in collisional orogens, (2) to investigate how deformation links both domains in space and time, and (3) to improve the understanding of the transition between the Asturian Massif and the Basque-Cantabrian Pyrenees.

2 Geological setting

The Biscay-Pyrenean domain is located between the southern North Atlantic and the Alpine Tethys (Tavani et al., 2018). This domain is subdivided into several segments that formed during an incomplete Wilson Cycle (Manatschal et al., 2021). The segments show a different rift maturity increasing westward, and a slightly to complete reactivation of the former rifted margin/rift system (Tugend et al., 2014). The geological evolution of this area is documented since the Palaeozoic with the Variscan orogeny (Martínez-Catalan et al., 2007; Matte, 1991). Subsequently, a post-Variscan extensional collapse preceded a multistage Mesozoic rifting, responsible for the formation of numerous extensional basins along northern Iberia (Roest and Sirvastava, 1991; Roca et al., 2011; Tugend et al., 2015; Cadenas et al., 2020; Frasca et al., 2021). The extensional evolution was complex, including three rift events: a first, distributed Triassic rifting that was accompanied by the uneven deposition of salt (Cámara and Flinch, 2017; Cámara, 2020; Gómez et al., 2007; López- Gómez et al., 2019), a Late Jurassic to Barremian transtensional rift event linked to narrow but deep depocenters aligned along the nascent and diffuse European-Iberian plate boundary (e.g., Asturian Basin, Cabuérniga Basin, Basque – Cantabrian Basin, etc.) (Cadenas et al., 2020; Tavani et al.,2018; Frasca et al., 2021; Miró et al., 2021), and a Late Aptian to Cenomanian hyperextended rift system that represents the main extensional event (Roca et al., 2011; Tugend et al., 2014; Pedreira et al., 2015; Cadenas et al., 2020; Miró et al., 2021; Lescoutre et al., 2021). As a result of the successive extensional phases, seafloor spreading took place in the Bay of Biscay while mantle exhumation occurred in the less mature North Iberian Rift System to the east (Tugend et al., 2014; Pedrera et al., 2017; García-Senz et al., 2019; Lescoutre et al., 2021). Thus, the segmentation of the North Iberian Rift System is the result of a long and complex evolution. Although the rifted margin configuration is fundamental to understand the reactivation and the subsequent evolution of the entire Pyrenean orogenic system during Late Cretaceous to Cenozoic (Muñoz, 1992; Roca et al., 2011; Tugend et al., 2014; Tavani et al., 2018; Frasca et al., 2021) it is not yet well understood in detail. Some first studies (Roca et al., 2011; Cadenas et al., 2020; Lescoutre and Manatschal, 2020; Saspiturry et al., 2020;

https://doi.org/10.5194/egusphere-2022-1175
Preprint. Discussion started: 18 November 2022

Lescoutre et al., 2021; Miro et al., 2021) addressed the study of the reactivation of the inherited rift structures. Here we make a step forward to understand the role of the rift inheritance to explain the along-strike structural changes in the Pyrenean orogen by means of an experimental approach based on scaled analogue (sandbox) models.

[Figure 1]

The present-day architecture of the entire Pyrenean orogen changes significantly along-strike due to the different tectono-sedimentary evolution and structural style (Fig. 1). The along-strike changes in the orogenic structure may although be one of the reasons of a confusing terminology (see Miró et al. (2020) for an overview). In this study we used: a) the Pyrenees *s.s.* for the eastern portion of the orogen where Mesozoic basins are located north and south of the Axial Zone, which is made of Paleozoic rocks representing the higher topography of the mountain belt; b) the Basque–Cantabrian Pyrenees for the central portion of the orogen characterized by the inversion of the Basque–Cantabrian Basin and surrounding minor basins, where Mesozoic rocks crop out, resulting in smoother topography; and c) the Asturian Massif for the western sector characterized by Paleozoic rocks with a very reduced Mesozoic succession on top but a significant topography to the south and a slightly reactivated extensional system offshore to the north (Fig. 1).

However, there are still many unanswered questions: How are the transitional domains connecting the different segments of the orogen? How do inherited rift structures control the contractional reactivation of the transitional domains? This work first addresses a generic problem, which is the along-strike transition from a salt-dominated segment to a segment controlled by basement structures without salt. Our study is inspired by the observations made along the southern transition between the Basque-Cantabrian and Asturian segments. We mainly focus on the proximal rift domains, which are the areas that never suffered a crustal thinning to less than 25 km thick (Tugend, et al., 2014, Cadenas et al., 2018) and their later reactivation during the Alpine Orogeny (Roca et al.,2011; Pedreira et al., 2015; García-Senz et al., 2019; Miró et al., 2021) (Fig. 2).

The Basque – Cantabrian Pyrenees are the result of the inversion of the western North Iberian hyperextended Rift System (Roca et al., 2011; Lescoutre and Manatschal, 2020; Cadenas et al., 2020; Miró et al., 2021). The hyperextension was controlled by a north dipping extensional detachment that was inverted during contraction. However, due to the salt detachment inherited from the Late Triassic rift event (López-Gómez et al., 2019; Lagabrielle et al., 2020), the reactivation of the Basque – Cantabrian Pyrenees occurred with a thin-skinned structural style, starting during the Late Cretaceous up to the Oligocene (Riba and Jurado, 1992; Tavani et al., 2013; Carola et al., 2013 and 2015; Cámara and Flinch, 2017; Cámara, 2020; Muñoz, 2019; Lescoutre and Manatschal, 2020; Miró et al., 2021). Consequently, the Mesozoic sedimentary succession of the southern Basque – Cantabrian Pyrenees has been transported over more than 30 km to the south over the foreland basin (Muñoz, 2019; Miró et al., 2021) (section 2, Fig. 2). As a result, salt structures developed in the thrust front have been reactivated and squeezed during inversion, whereas the ones located to the north into the thrust wedge (i.e., Alavesa Platform) and developed in more distal domains (northern part of the former rift proximal domain and its transition

https://doi.org/10.5194/egusphere-2022-1175
Preprint. Discussion started: 18 November 2022

to the necking domain) are still preserved showing none, or slightly, contractional reactivation (e.g., Salinas del Rosio and Villasana de Mena salt diapirs) (section 2, Fig. 2). The underlying basement is flat in the Duero and Ebro foreland basins whereas slightly dips northward beneath the frontal thrust (Carola et al., 2015; Muñoz, 2019; Miró et al. 2020 and 2021). Other interpretations have been proposed for the Basque – Cantabrian Pyrenees arguing for a thick-skinned reactivation with no decoupling along the Triassic salt (Quintana et al., 2015; Pedrera et al., 2017 and 2020; García-Senz et al., 2019).

[Figure 2]

In the Asturian Massif, on the contrary, a consensus exists on the interpretation of the Pyrenean contractional structures. In this area, they consist of a thick-skinned thrust system controlled by the reactivation of previous Variscan faults (Alonso et al., 1996; Gallastegui, 2000). Triassic salt was either not deposited or completely eroded (López-Gómez et al., 2019) conditioning the thick-skinned structural style. Thus, the area shows a contrasting structural style compared to the Basque – Cantabrian Pyrenees further to the east. The proposed interpretations of the Asturian Massif (e.g., Alonso et al., 1996, Pulgar et al., 1999) show a major mid-crustal sole thrust dipping to the north and being flat at about 20 km depth acting as an intra-crustal decoupling level for the structures depicted in the hanging wall (section 1, Fig. 2). The fault propagation fold observed at the thrust front involving the Paleogene-Neogene syn-orogenic sediments located at the northern limit of the Duero Basin represents the field expression of this major sole thrust (Pulgar et al., 1999; Gallastegui, 2000).

In between, a less investigated domain connects the Asturian domain to the west with the Basque – Cantabrian domain to the east (Fig. 2). The transitional domain is characterized by both E-W (e.g., Cabuérniga Fault) and NW-SE (e.g., Rumaceo and Golobar Faults) major structures that outcrop to the west but sole out to the east, plunging eastwards. These inherited basement-involved structures (Espina, 1996) have been reactivated during both rifting and orogenic phases. In addition, the Upper Triassic salt has an irregular distribution in this transitional domain, being abundant to the north in the Santander Block, with little or no evidence in the Cabuérniga Basin but outcropping again to the south in the Polientes Basin (López-Gómez et al., 2019). Moreover, salt thickness increases to the east (Camara, 2017). Early Cretaceous extensional faults and related salt structures and Lower Cretaceous minibasins are observed in this domain (García de Cortázar and Pujalte, 1982; Espina, 1994). However, besides some good outcrops, vegetation, poorly imaged and scarce seismic, and drill hole data, which is very poor or absent in most of the transitional domain, makes precise and further investigation difficult and complex.

https://doi.org/10.5194/egusphere-2022-1175
Preprint. Discussion started: 18 November 2022

3 Analogue modelling

3.1 Experimental methodology

3.1.1 Model set-up

The experimental configuration simulates: 1) the distribution of basement-involved structures, aiming to reproduce the inverted extensional faults at the western edge of the Asturian Massif (i.e., Cabuérniga and Golobar-Rumaceo faults, Fig. 2), and 2) an uneven distribution of the Upper Triassic salt (Keuper), aiming to reproduce a thick salt layer in the Basque-Cantabrian Pyrenees pinching out towards the Asturian Massif (Fig. 3).

According to that, the 3D experimental program was carried out in a 75 cm-long, 70 cm-wide glass-sided deformation box (Fig. 3a). Two mobile end walls orthogonal to the glass-sided walls made the experiment a closed system. Both glass walls were fixed whereas computer-controlled servomotors moved the two metal ones. Two rigid wooden blocks attached to the mobile end walls were used to simulate the inherited basement structures (Figs. 3a and b). Both blocks have a regional dip of 3° to the E. The northern block had a rectangular plan view shape whereas the southern one was trapezoidal (Figs. 3a and b). In both cases, a surface dipping 60° towards the inner part of the model simulated the E-W Cabuérniga Fault (northern block) and the NW – SE Golobar and Rumaceo Faults (southern block) (Figs. 3a, b, and e). The space between the two blocks was filled with white silica sand keeping the 3° eastwards regional dip. Then, a purple sand layer wedging eastwards as the previous materials overlie both blocks and the white sand.

On the other hand, the two rigid blocks changes to two flat wooden plates on the eastern side of the rig (Figs. 3a and b). Here, a 19 mm-thick polymer layer pinching out westwards on top of the basement sand wedge simulates the Upper Triassic salt basin at the Basque-Cantabrian Pyrenees (Figs. 3c and d). It has been estimated that the original thickness of the Upper Triassic evaporites is between 500 and 2000 m throughout the basin (Cámara and Flinch, 2017). Finally, a 10 mm-thick blue sand layer overlaid the polymer layer pinching out westwards against the basement wedge (Figs. 3c, d, and e). According to the polymer distribution, three structural domains can be defined: a) a western coupled domain without polymer; b) a central transitional domain where the polymer overlaps the basement blocks; and c) an eastern decoupled domain where the thickness of the polymer is constant (Fig. 3d). These structural domains will be hereinafter used to facilitate the explanation of the experimental results.

[Figure 3]

3.1.2 Analogue materials and scaling

Well-sorted and rounded dry silica sand was used as analogue for brittle rocks in the upper continental crust (Schellart, 2000). On the other hand, a polydimethylsiloxane (PDMS) silicone polymer simulated the behaviour of viscous salt (Weijermars, 1986; Dell'Ertole and Schellart, 2013). The silica sand (white or coloured) with an average grain size of 199

https://doi.org/10.5194/egusphere-2022-1175
Preprint. Discussion started: 18 November 2022

μm obeys a Mohr-Coulomb criterion of failure (Hubbert, 1951; Mandl et al., 1977). The mechanical properties of the poured sand were determined by Roma et al. (2018a) by means of a shear box test, resulting in 34.6° of internal friction, 1500 kg·m^{-3} bulk density, 0.69 of internal friction coefficient, and a low apparent cohesive strength of 55Pa. The PDMS is a near-Newtonian viscous fluid with a density of 972 kg·m^{-3}, a viscosity of 1.6×10^{-4} Pa, and a strain range of 1.83×10^{-4}cm·s^{-1} at 20°C (Dell'Ertole and Schellart, 2013). The mechanical properties of the analogue materials and the scaling factors of the experimental program are summarised in Table 1.

Table 1. Scaling parameters used in the experimental program

Parameter	Experiment	Nature	Ratio
Length (m)	0.01	1000	10^{-5}
Density sand (Kg·m^{-3})	1500	2700	0.55
Gravity acceleration (m·s^{-2})	9.81	9.81	1
Density polymer (Kg·m^{-3})	972	2200	0.44
Viscosity polymer (Pa·s)	$1.6\cdot10^{4}$	10^{18} - 10^{19}	$1.6 \times 10^{-14/-15}$

Table 1: Scaling parameters used in the experimental program.

3.1.3 Procedure

The experimental program presented in this work includes three different experiments (Table 2). Model-1 corresponds to the baseline model in order to understand what the structural grain was at the end of the extensional episode. Model-2 and Model-3 followed the same extensional evolution than Model-1, but then they were inverted (Table 2). Syn-inversion sedimentation was considered in Model-3 (Table 2).

Table 2. Experimental program

Experiment	Total extension *(mm)*	Extension rate *(mm/h)*	Total shortening *(mm)*	Shortening rate *(mm/h)*	Syn-comp. sedimentation	Time *(hours)*
Model - 1	127	3 (N wall) 2 (S wall)	-	-	-	31
Model - 2	127	3 (N wall) 2 (S wall)	200	6 from N 0 from S	-	64
Model - 3	127	3 (N wall) 2 (S wall)	200	6 from N 0 from S	Yes	68

Table 2: Experimental program presented in this work.

The extensional deformation was achieved by moving the two end walls by a servomotor-driven worm-screw controlled by a computer. In order to produce more accommodation space to the north, where the main depocenter was in the Basque-Cantabrian Basin, the northern wall pulled at a higher velocity (3mm/h) than the southern one (2mm/h). Interbedded layers of white and red sand were used to simulate syn-extensional sedimentation. To favour the early development of salt

https://doi.org/10.5194/egusphere-2022-1175
Preprint. Discussion started: 18 November 2022

structures, the first syn-extensional sand layer was poured after 5 hours of extension. All subsequent syn-extensional sand layers were settled every 3 hours. Before the sedimentation of each syn-extensional layer, the rig was tilted 0.35°northwards to simulate the progressive tilting of an extensional rifted margin reaching a regional dip of 2.8° at the end of the extensional phase. At the end of Model-1, the total extension was 127mm (Table 2), (75mm for the northern end wall and 52mm for the southern one), and the resulting basin was filled by 8 syn-extensional sand layers.

After the extensional episode, Model-2 and Model-3 were covered by a 5mm-thick yellow sand layer simulating a post-extensional unit. Both models were subsequently shortened by pushing the northern end wall at a velocity of 6mm/h during 38 hours reaching 200 mm of total shortening. Syn-inversion sedimentation was only considered for Model-3 (Table 2) by alternating green and white sand layers every 3 hours. In addition, after the deposition of each syn-compressional sand layer, the rig was tilted 0.2° to the north up to additional 2.2° to simulate the orogenic flexure of the Basque – Cantabrian Pyrenees (Fig. 2).

4 Experimental results

This chapter describes the experimental results of the three models pointing out the kinematics of each deformation phase. Model-1 focuses on the extensional evolution and allows to understand the role of stratigraphic and structural inheritance during the rift phase (Table 2). Model-2 and Model-3 underwent an extensional evolution similar to Model-1 but were subsequently shortened to study how inherited extensional structures were inverted (Table 2). In addition, Model-3 also explores the role of syn-contractional sedimentation during inversion (Table 2). The description of each model has been addressed according to the deformation style of the coupled, transitional, and decoupled structural domains previously introduced (Figs. 3c and d).

4.1 Model-1

Model-1 corresponds to the baseline experiment performed to understand the main extensional elements. During early extension, the experiment shows a strong control of the rigid wooden blocks in the coupled domain, where an E-W trending graben develops over the edge of the northern block, and a NW–SE trending graben over the southern one (Fig. 4a). In contrast, any structure formed in the decoupled and transitional domains. As extension increases, the northern E-W graben of the coupled domain widens controlled by a major normal fault rooted at the edge of the rigid block to the north, and a set of two antithetic faults developed to the south (Fig. 4b). Similarly, the southern graben also widens but only a single antithetic fault developed due to the lower extension rate (Fig. 4b). After 25 mm of extension, a wide salt inflation occurred in the central area of the decoupled domain separating two E-W trending grabens at the northern part of the basin and two at the southern one of (Fig. 4b). Triggered by thin-skinned extension, such grabens developed at the top of reactive salt walls

https://doi.org/10.5194/egusphere-2022-1175
Preprint. Discussion started: 18 November 2022

evolving to active with increasing extension (Vendeville and Jackson, 1992a). In the transitional domain, however, four minor grabens relay the two major thick-skinned structures of the coupled domain and the thin-skinned structures of the decoupled domain (Fig. 4b).

240

[Figure 4]

Further extension widens the two grabens of the coupled domain by generating new antithetic normal faults (Figs. 4c and 5a). Progressive northwards tilting of the model during the extensional episode triggered gravitational gliding in the 245 decoupled and transitional domains, where the bounding grabens evolve to asymmetric half-grabens controlled by downdip faults (Figs. 5b and 5c). The active salt walls of the decoupled domain evolved to passive diapirs producing small overhangs (Vendeville and Jackson, 1992a; Jackson et al., 1994; Rowan and Giles, 2020) (Figs. 4c and 5c). The wide salt-cored anticline developed at the central position of the decoupled domain is progressively inflated as offlap terminations of the syn-kinematic sand layers indicate (Figs. 4c and 5c). In the meantime, in the transitional domain, the grabens related to the 250 northern structure of the coupled domain were buried and extensional deformation was accommodated in a footwall breached relay ramp linking the northern passive salt wall of the decoupled domain (Fig. 4c). Similarly, a footwall breached relay ramp linked the southern graben of the coupled domain with the southern passive salt wall of the decoupled domain (Fig. 4c).

255 **[Figure 5]**

From 70 to 115 cm of extension, the two grabens of the coupled domain widened, and new antithetic faults developed (Figs. 4d and 5a). In the decoupled domain, polymer extrusion at the northern passive salt wall ended after 80 mm of extension when the source layer depleted, and primary welds developed. From this point, the northern salt wall became progressively 260 buried by syn-kinematic sedimentation (Figs. 4d and 5c). Further extension widened the diapir producing the roof collapse and the development of a graben (diapir fall sense Vendeville and Jackson, 1992b) (Figs. 4d and 5c). In contrast, the flaring upwards geometry of the southern passive salt wall indicates that extrusion took place until the end of the extension when primary welds developed (Fig. 5c). In the meantime, a graben develops in the crest of the salt-inflated anticline between the two salt walls (Fig. 4d) that will be pierced by polymer developing a new passive salt wall at the last stages of extension 265 (Fig. 5c). Part of the extensional deformation also shifted to the southern polymer pinch out where a regional dipping extensional fault developed (Fig. 5c). During this episode of deformation, the E-W grabens of the transitional domain become inactive and buried (compare their position in Figs. 5c and 5d). Two new oblique (NW–SE), transtensional grabens developed linking the major grabens of the coupled domain with the new central graben of the salt-inflated anticline and the regional dipping fault developed at the southern polymer pinch out of the decoupled domain (Fig. 4d). Coeval to the

https://doi.org/10.5194/egusphere-2022-1175
Preprint. Discussion started: 18 November 2022

formation of the southern transtensional oblique graben, there was a switch in the depocenters location (flip-flop salt tectonics sensu Quirk and Pilcher, 2012). Growth strata clearly indicates that the older depocenter is controlled by the growth of the counter-regional fault. Once the hanging wall of this fault touched down forming a weld, there was a switch of the deformation to the new major regional dipping fault at the southern oblique graben. This change is recorded by a polarity change of growth strata related to both faults, and by the development of an intermediate unconformity (Fig. 5b).

4.2 Model-2

Model-2 followed the same extensional evolution as Model-1, but it was subsequently inverted without syn-contractional sedimentation (Table 1). To avoid repetitions, this section will focus on the description of the results related to the contractional evolution of this model only.

At the end of the extensional episode, the entire model was covered by a 5 mm-thick post-extensional yellow sand layer burying the extensional structures and diapirs. During the onset of shortening, deformation concentrated at the closest structures to the moving wall in the coupled domain. The northern graben in the coupled domain was folded and uplifted by the inversion of the northern master extensional fault and the formation of a foreland-directed thrust nucleated at the base of the rigid bock (Figs. 6a and 7). Inversion of the northern graben and its master fault continued into the transitional domain. Moreover, the minor E-W graben and related reactive diapir at the southern edge was also reactivated (compare Figs. 4c, 5a and 6a). In the decoupled domain, shortening progressed further south rejuvenating both the northern and southern salt walls by squeezing, folding and uplifting their roofs (Fig. 6a). Salt pierced the roof at the eastern sector of the northern salt wall and extruded forming a salt sheet (Fig. 6a). During early inversion, the location of the thrust front is constrained by the pre-existing extensional faults and salt structures. It has a W-E trend in the coupled domain and slightly shifts southwards in the decoupled domain. At the transitional domain, both thrust fronts overlap in a soft linkage relaying thick- and thin-skinned domains respectively (Fig. 6a). Part of the contractional deformation propagated to the southern salt wall in the decoupled domain as seen by the salt inflation. Deformation decreases laterally along the intermediate domain, being null in the equivalent coupled domain (Fig. 6a).

[Figure 6]

In further stages of shortening, the height of the northern inverted graben at the coupled domain increases by the emplacement of south-verging thrusts in a piggy-back sequence, but also by the footwall shortcut that develops at the northern edge of the graben (Figs. 6b and 7a). In the decoupled domain, the buried northern salt wall narrows, increasing roof uplift and folding (Fig. 7c). At the eastern termination, the extruding polymer forms a salt sheet that flows down the limbs of the resulting anticline (Fig. 6b). Contractional deformation reaches the southern pinch-out of the salt basin where an E-W trending foreland-verging thrust developed. The extrusion in the southern salt wall notably increased resulting in a large

https://doi.org/10.5194/egusphere-2022-1175
Preprint. Discussion started: 18 November 2022

piggy-back salt sheet confined by the different contractional structures (Fig. 6b). The salt-cored anticline located between the two salt walls is progressively amplified with increasing shortening. The structural complexity of the transitional domain increases as deformation evolved. The northern E-W trending thrust front becomes rectilinear, linking the foreland-verging thrust of the coupled domain with the foreland-directed thrust nucleated at the top of the buried northern salt wall (Fig. 6b). Further south, the structural style of the transitional domain is strongly controlled by salt thickness. The E-W trend of the decoupled domain structures progressively curves into a NW-SE trend (Fig. 6b). A tear fault developed at the western edge of the salt basin linking the deformation front of the decoupled and coupled domains and segmenting the thrust sheets (Fig. 6b. Southwards of this structure, the E-W trending thrust at the pinch out of the salt basin progressively curves to reach a NW-SE trend in the transitional domain (Fig. 6b).

Increasing shortening forced the rise of a prominent topography in most structures. The southern salt wall of the decoupled domain becomes progressively squeezed developing a secondary weld around 80 mm shortening (Figs. 6c and 7c). After welding, contractional deformation switch from the southern thrust front to the salt-cored anticline northwards of the southern salt wall. This structure is progressively amplified first by buckling and then by the development of a thrust in its southern limb and a back thrust in the northern one (Figs. 6c and 7c). In addition, the southern limb of the anticline experienced a progressive limb rotation, most probably due by a higher friction on the primary weld underneath the secondary one (Figs. 6c and 7c). After 138 mm of shortening the oblique southern graben at the coupled domain is inverted. This is coeval with a continuous slight clockwise vertical axis rotation of the structures at the transitional domain and an increase of the thrust curvature (compare Figs. 6b and 6c). New tear faults trending parallel to the shortening direction develop close to the polymer pinch out at the transitional domain.

From this point until the end of the experiment, shortening amplifies previous structures. In the coupled domain, the orogenic wedge favours the propagation of contractional deformation towards the foreland with the initial inversion of the southern oblique graben, which is subsequently cut out of sequence by the floor thrust of the northern foreland-directed thrust system (Figs. 6d and 7a). In the decoupled domain, shortening amplified the salt-cored anticline developing a crestal collapse graben (Figs. 6d and 7a). During the last stages of deformation, the frontal thrust is reactivated (Fig. 6d). In the transitional domain, contractional deformation is mainly accommodated by the thrust that nucleates at the apex of the reactive diapir inherited from the previous extensional episode (Fig. 4b). This structure links the salt-cored anticline of the decoupled domain with the frontal thrust of the coupled domain (Fig. 6d). At the northwards sector of the transitional domain, there is also a significant uplift of the graben because of the pre-salt impinging into the overburden (coupled deformation). Part of the deformation is absorbed by the reactivation of the inherited primary weld as a thrust weld.

[Figure 7]

https://doi.org/10.5194/egusphere-2022-1175
Preprint. Discussion started: 18 November 2022

4.3 Model-3

The kinematic evolution of Model-3 during the extensional episode was similar to Model-1 and Model-2, but in this case, sedimentation was introduced during the inversion episode (Table 1). In order to avoid repetitions, this section will address the most remarkable differences due to syn-inversion sedimentation.

Despite syn-kinematic sedimentation, the contractional evolution of the three structural domains during early shortening is like in Model-2 (compare Figs. 6a and 8a). The most outstanding differences occur after 70 mm shortening, when syn-contractional sedimentation inhibits the propagation of deformation at the southern salt pinch out as it occurs in Model-2. In this case, shortening is accommodated by the salt-cored anticline northwards of the southern salt wall (Fig. 8b), which for a similar shortening rate reaches a higher topographic relief (Figs. 6b and 8b). The buttressing produced by secondary welding together with the syn-kinematic sedimentation triggered a backthrust, resulting into a more asymmetric anticline than in Model-2 (Figs. 7c and 9c). A new diapir pierces the roof of the northern salt wall that progressively thins by crestal extension as fold growths. The structure of the transitional domain is also slightly different from that of Model-2. The main structure resulted from the westward propagation of the central salt-cored anticline instead of the reactivation of the oblique grabens. The thrust related to this anticline linked with the frontal thrust of the coupled domain along a N-S trending tear fault. (Fig. 8b). In the coupled domain, the oblique southern graben and its propagation towards the transitional domain were rapidly buried by syn-contractional sedimentation without any apparent inversion (Fig. 9b).

[Figure 8]

During the subsequent stages of compression, the major structures of the model are barely amplified. A crestal collapse graben develops in the salt-cored anticline of the decoupled domain (Figs. 8c and 8d). The thrusts emplaced in a piggy-back sequence between 138 and 200 cm of shortening at the coupled domain overthrust the southern graben inhibiting their inversion. New diapirs pierce the crest of the central anticline thinned by a crestal collapse graben at the decoupled domain. Likewise, the volume of polymer at the salt sheets at the end of the experiment is less than in Model-2. The final section of the decoupled domain (Fig. 9c) shows that the northern salt wall is practically welded at the end of the experiment. This fact triggered a greater upwards polymer flow raising and folding the roof, where an incipient crestal collapse graben developed (Fig. 9c).

[Figure 9]

https://doi.org/10.5194/egusphere-2022-1175
Preprint. Discussion started: 18 November 2022

5 Discussion

5.1 Thick- to thin-skinned transition of the extensional system

Controlled by the experimental setup that includes a western domain with two basal rigid blocks and a décollement layer in the eastern domain, the final structural style shows significant differences along-strike. The coupled domain is characterized by a thick-skinned deformation constrained by the rigid blocks that control the inherited extensional structures' reactivation during the inversion episode. These two blocks simulate E-W and NE-SW-trending basement-involved faults. On the contrary, the decoupled domain, constrained by a salt-equivalent layer underneath the brittle succession, shows a thin-skinned deformation, characterized by E-W-trending structures either during the extensional and subsequent inversion episodes. In addition, our models are new in the sense that they show the linkage between the structures of the coupled and the decoupled domains along a transitional domain with a progressive thinning of the salt horizon, and how the inherited extensional structural grain controls the location of the contractional structures.

During the early extension, the structures developed in the transitional domain are nucleated at the intersection between the edges of the rigid blocks and the polymer pinch out (Fig. 4b). However, their orientation follows the structural trend of the decoupled domain. This result confirms that even a thin weak horizon may promote decoupling from the inherited basement features, regardless they may control the location of the suprasalt structures. The location of the structures in the transitional domain results from the linkage of the structures in the adjacent domains (Fig. 4c). Structures in the coupled domain are imposed by the basement-involved faults, as reproduced by the fixed wooden blocks. However, the location of the structures in the decoupled domain depends on the ratio overburden/salt thicknesses, the position of the salt pinch-out, and the syn-tectonic sedimentation. As a result, structures in the decoupled domain extend further and the absence of collinearity with the structures in the coupled domain results into the development of stepped relay ramps in the transitional domain connecting parallelly-oriented grabens of the other domains (Figs. 4b and 4c).

Primary welding by salt evacuation in the decoupled domain has a critical impact on the location of new structures as extension increased. Consequently, it affects the trend of the younger extensional faults in the transitional domain. Their orientation depends on the linkage between the active structures of the decoupled and coupled domains (Fig. 4d). Welding of the basins adjacent to the salt wall in the decoupled domain promoted the migration of the deformation toward the pinch out of the salt layer as well as the collapse of the central salt pillow and related salt wall (Fig. 4d). These newly formed extensional faults, which are in a different position than the former ones, tend to link with the reactivated basement-involved fault at the coupled domain, which remains in a fixed position. As a result, new extensional faults with an oblique trend form in the transitional domain. Such oblique grabens could be misinterpreted as a subsalt N-S trending strike-slip fault with a dextral displacement.

https://doi.org/10.5194/egusphere-2022-1175
Preprint. Discussion started: 18 November 2022

5.2 Thick- to thin-skinned transition during inversion

Two distinct inversion tectonic styles developed in the coupled and decoupled domains as controlled by the reactivation of basement-involved faults and the reactivation of extensional and salt structures respectively. The coupled domain is characterized by a thrust system nucleated in the major extensional faults and a high structural relief given the absence of a weak horizon at the bottom of the thrust wedge. The thin-skinned structural style in the decoupled domain is mainly controlled by the thickness and distribution of salt as well as the location of the salt structures and the extensional faults that triggered them. Synchronous thrusting into the thrust wedge occurred in both domains, although in the decoupled domain the thrust sequence was also controlled by the primary welding of the salt layer as well as by the secondary welding once salt structures were squeezed.

During the contractional deformation, the transitional domain is again the area where oblique and transverse structures develop. However, unlike what occurs in the extensional event, a hard linkage zone developed during the inversion since the early stages of deformation, characterized by N-S trending faults connecting the frontal structures of the coupled and decoupled domains (Figs. 6, 8, and 10).

The inherited salt structures of the decoupled domain are the first to experience contractional deformation at the early stages of inversion synchronously with the inversion of the northern graben of the coupled domain. Buried diapirs are contractionally rejuvenated, squeezed and their overburden folded and uplifted as the inversion of the northern graben of the coupled domain continued (Figs. 6 and 8). In the transitional domain, the first structures to develop are the ones related with the reactivation of the relay grabens and related diapirs synchronously with the reactivation of the master fault of the northern graben. Immediately afterwards, active structures in the decoupled and coupled domains link, forming N-S trending structures in the transitional domain. This transverse linkage occurs connecting active structures and shows different extent and evolution depending on their location, which in their turn is controlled by the inherited extensional and related salt structures and the syn-tectonic sedimentation. Thus, in the model with syn-orogenic sedimentation, the N-S trending element is shorter, as the sy-ntectonic sedimentation inhibits the forward propagation of the deformation. In addition, it shows a simpler structure than model-2 without syn-orogenic sedimentation (compare Figs. 6 and 8). In model-2, the transverse structures consist of two opposed verging thrust salients dissected by a N-S fault, whereas in model-3, a more continuous trending structure developed (compare Figs. 6b and c with Figs. 8b and c). Moreover, in model-2, where deformation progressed forwards both in the decoupled domain (reactivation of the salt pinch out at the thrust front) and in the coupled domain (inversion of the oblique southern graben), the newly formed structures linked also into the transverse N-S system (Fig. 6). Such evolution results into a significant along strike change of this system. Thus, in model-3, the transverse structural element consists of a pop-up bounded by high-angle thrusts in the northern part, whereas further south it corresponds of a shallow dipping thrust with a hanging wall ramp moderately dipping to the west. Such variation occurs in a very short distance along a continuous structure at surface that could be interpreted as a strike-slip fault (Fig. 10). Thus, a section trough the northern part of the N-S structural element could be interpreted as a flower structure (Figs. 10f and 12d

https://doi.org/10.5194/egusphere-2022-1175
Preprint. Discussion started: 18 November 2022

and f), whereas the southern edge of the structure corresponds to a lateral ramp of a south-directed thrust linked to the central structure of the decoupled domain (Figs. 10g and 12c and e).

[Figure 10]

Structures with an initially opposed vergence can link resulting into a single structure with an along-strike change of vergence. An example is the central salt-cored anticline of the decoupled domain that linked with the inverted southern relay graben and related reactive diapir of the transitional domain in both models 2 and 3 (Figs. 6, 8 and 11). The backthrust at the northern limb of the central salt-cored anticline evolves to a pop-up at the boundary between the decoupled and transitional domains and to a forward verging structure into the transitional domain (Fig. 11).

The impact of the syn-contractional sedimentation on the structural evolution of the transitional domain is also notable. Whereas in the model-2 structures striking NW-SE are developed during the early stages of contraction being later crosscut by N-S strike-slip faults (Fig. 6), in model-3 the active structures in both surrounding domains are in a different position resulting in a simpler evolution as explained above governed by N-S orientations.

Thus, the combination of: (1) the location of the inherited salt structures, developed during the extensional episode, and (2) the syn-inversion sedimentation, controlling the location of the active structures in the decoupled domain, determined the orientation and location of the structures at the transitional domain.

[Figure 11]

5.3 Comparison to the Asturian Massif and Basque – Cantabrian Pyrenees

A first order correlation between the models presented in this work and the Asturian and Basque – Cantabrian domain is the regional east plunging structural trend observed in both cases. The Asturian Massif presents higher topography and a narrower deformation zone as it occurs in the western part of the model. Following the Coulomb-wedge theory, the higher basal friction due to the lack of an efficient decoupling level, allows to support more relief. On the contrary, the Basque – Cantabrian Pyrenees present a lower topography and a wider area of deformation as observed in the eastern part of the model. This is due to the presence of an efficient decoupling horizon (i.e., salt) at the base of the sedimentary succession. Therefore, even if the similarity of the model with the observations cannot be used as a proof to support the interpretation proposed here, it shows that the existence of a salt/decoupling horizon may be a prerequisite to obtain the final structures and architecture observed. This experimental program, as such, is in line with the interpretation of the Basque – Cantabrian Pyrenees as thin-skinned system in contraposition to other models totally controlled by thick-skinned structures (Quintana et al., 2015; Pedrera et al. 2017, 2020; García-Senz et al., 2019).

https://doi.org/10.5194/egusphere-2022-1175
Preprint. Discussion started: 18 November 2022

The transitional domain between the thick-skinned Asturian Massif and the thin-skinned Basque – Cantabrian Pyrenees is characterized by the presence of numerous oblique and transversal structures, as revealed in our models. The main structures in the transitional domain trend mostly N-S to NW-SE and are not consistent with a transpressive inversion model with a NW-SE shortening direction (Tavani et al., 2013). Even more, as shown by the models with the presence of a salt boundary, such structural trends do not require a reactivation of a regional basement transfer feature. In detail, the structures observed in the transitional domain between the Asturian Massif and Basque – Cantabrian Pyrenees are more complicated than the ones reproduced in our models, mainly resulting from the intricate geometry of the Triassic and Late Jurassic-Early Cretaceous rift systems that developed in the area and controlled the distribution of the Triassic salt (López-Gómez et al., 2019, Miró et al., 2021). However, some striking similarities are observed. The Pas thrust system, oriented NW-SE to N-S, connects the western edge of the salt inflated area located north of the Plataforma Burgalesa with the inverted Cabuérniga extensional fault system, where the basement is involved. The hanging wall of the Pas thrust shows a pop-up structure as also revealed by our models (Figs. 9b and 10f). It involves the basement of the transitional domain that has been thrust on top of the coupled domain as partially shown in our models (Fig. 9b). In the section of Fig. 10f the Pas thrust would correspond with the western thrust of the pop-up at the boundary between the transitional and coupled domains. Regardless that in this section it is not the main thrust, it may change along-strike bringing the subsalt succession on top of the salt layer as observed in other sections (Fig. 9b). Along-strike changes of vergence in the transitional and decoupled domains is another feature reproduced in the models and observed also in the field case study (Figs. 9, 11 and 12). Other oblique features are observed further south in the transitional domain between the Asturian Massif and the Basque-Cantabrian Pyrenees (Fig. 2). They also connect the former salt walls or salt inflated areas located along the southern edge of the Plataforma Burgalesa and the present thrust front with the inverted basement-involved faults of the Asturian massif.

[Figure 12]

A second aspect related to the previous one is the distribution of syn-contractional sedimentation. Whereas in the Asturian Massif (i.e. coupled domain) the syn-contractional sedimentation occurred exclusively in the foreland Duero Basin due to the orogenic wedge development to the north (Figs. 11c and d) (Pulgar et al., 1999; Alonso, 2007), in the Basque – Cantabrian Pyrenees (i.e. decoupled domain) the distribution of deformation favoured a more distributed topography and therefore a more distributed syn-contractional deformation both in the foreland basin but also in the piggyback basins between the main salt structures (Muñoz, 2019; Miró et al. 2021) (Fig. 11e and f). In between, minor basins with triangular shapes partially controlled by thick-skinned and thin-skinned structures are located (e.g., Cabuérniga and Polientes basins).

https://doi.org/10.5194/egusphere-2022-1175
Preprint. Discussion started: 18 November 2022

6 Conclusions

Using an analogue modelling experimental approach, the aim of this study is to investigate the distribution and evolution of deformation in a thick- to thin-skinned along-strike transition inherited from a rift system during subsequent inversion. The experimental setup has been inspired by observations made in the transition from the autochthonous Asturian Massif to the allochthonous Basque-Cantabrian Pyrenees.

The experimental program presented here demonstrates that the trend and kinematics of oblique structures developed in the transition between domains with and without salt depend on the evolution of active structures in the surrounding thick- and thin-skinned domains. But more importantly, the fact that even a thin low frictional horizon (i.e. the lateral salt pinch–out) may significantly control the structural trend in such positions. The structures in the transitional domain formed by the progressive soft- to hard-linkage of the ones developed in the adjacent domains, which resulted into apparent along-strike changes of geometry and vergence.

Therefore, the experimental results point out the importance of the inheritance: either structural by considering the distribution and orientation of pre-existing basement-involved faults, but also compositional related to the presence and distribution of effective decollement levels. Both aspects have a strong impact on the subsequent contractional evolution of the transitional domain, and the misinterpretation of one of them can introduce significant uncertainties unrevealing the presalt geometry.

Finally, the experiments confirm the thick-skinned style controlling the reactivation of the Asturian Massif by creating a narrow thrust wedge with high topography and syn-contractional sediments deposited in the foreland. On the other hand, the models show a wider deformed area to the east with salt structures but with less topographic relief due to the effectiveness of the salt decoupling. This sector is characterized by a more distributed syn-contractional sedimentation both in the foreland and in the deformed domain, similar to what is observed in the Basque – Cantabrian Pyrenees case study.

Acknowledgments

We acknowledge the support of the research project Structure and Deformation of Salt-bearing Rifted Margins (SABREM), PID2020-117598GB-I00, funded by MCIN/ AEI /10.13039/501100011033 and the OROGEN research project. The GEOMODELS Research Institute and the Grup de Geodinàmica i Anàlisi de Conques (2017SGR-596) are also acknowledged for their financial support. The experimental program presented in this work was carried out at the Geomodels Analogue Modelling Laboratory, a Scientific Infrastructure co-funded by the European Regional Development Fund of the Ministerio de Ciencia e Innovación of the Spanish Government (UNBA08-4E-006). We also thank P. Granado, O. Gratacós, M. Snidero, M. Roma, O. Pla, and F. Escosa for logistical support in the modelling laboratory.

https://doi.org/10.5194/egusphere-2022-1175
Preprint. Discussion started: 18 November 2022

References

Acocella, V., Salvini, F., Funiciello, R., and Faccenna, C.: The role of transfer structures on volcanic activity at Campi Flegrei (Southern Italy), J. Volcanol. Geoth. Res., 91(2-4), 123-139, https://doi.org/10.1016/S3077-0273(99)0032-3, 1999.

Alonso, J., Pulgar, J., García-Ramos, J., and Barba, P.: Tertiary basins and Alpine tectonics in the Cantabrian Mountains (NW Spain), in: Tertiary Basins of Spain: The Stratigraphic Record of Crustal Kinematics, edited by: Friend, P.F., Dabrio, C.J., Cambrigde University Press, Cambridge, UK, 214-227, https://doi.org/10.1017/CBO9780511524851, 1996.

Alonso, J., Pulgar, J., and Pedreira, D.: El relieve de la Cordillera Cantábrica. Revista de la Asociación Española para la Enseñanza de las Ciencias de la Tierra, 15(2), 151-163, 2007.

Amilibia, A., McClay, K.R., Sàbat, F., Muñoz, J.A., and Roca, E.: Analogue modelling of inverted oblique rift systems. Geol. Acta, 3(3), 251-271, https://doi.org/10.1344/105.000001395, 2005.

Amilibia, A., Sàbat, F., McClay, K.R., Muñoz, J.A., Roca, E., and Chong, G.: The role of inherited tectono-sedimentary architecture in the development of the central Andean mountain belt: Insights from the Cordillera de Domeyko. J. Struct. Geol., 30(12), 1520-1539. https://doi.org/10.1016/j.jsg.2008.08.005, 2008.

Bahroudi, A., and Koyi, H.: Effect of spatial distribution of Hormuz salt on deformation style in the Zagros fold and thrust belt: an analogue modelling approach. J. Geol. Soc. London, 160(5), 719-733, https://doi.org/10.1144/0016-764902-135, 2003.

Beaumont, C., Muñoz, J.A., Hamilton, J., and Fullsack, P.: Factors controlling the Alpine evolution of the central Pyrenees inferred from a comparison of observations and geodynamical models. J. Geophys. Res-Sol. Ea., 105(B4), 8121-8145, https://doi.org/10.1029/1999JB900390, 2000.

Bonini, M., Sani, F., and Antonielli, B.: Basin inversion and contractional reactivation of inherited normal faults: A review based on previous and new experimental models. Tectonophysics, *522*, 55-88, https://doi.org/10.1016/j.tecto.2011.11.014, 2012.

Butler, R.W., Tavarnelli, E., and Grasso, M.: Structural inheritance in mountain belts: an Alpine–Apennine perspective. J. Struct. Geol., 28(11), 1893-1908, https://doi.org/10.1016/j.jsg.2006.09.006, 2006.

Cadenas, P., Fernández-Viejo, G., Pulgar, J. A., Tugend, J., Manatschal, G., and Minshull, T.A.: Constraints imposed by rift inheritance on the compressional reactivation of a hyperextended margin: Mapping rift domains in the North Iberian margin and in the Cantabrian Mountains. Tectonics, 37(3), 758-785, https://doi.org/10.1002/2016TC004454, 2018.

Cadenas, P., Manatschal, G., and Fernández-Viejo, G.: Unravelling the architecture and evolution of the inverted multi-stage North Iberian-Bay of Biscay rift, Gondwana Res., 88, 67-87, https://doi.org/10.1016/j.gr.2020.06.026, 2020.

Cámara, P.: Inverted turtle salt anticlines in the eastern Basque-Cantabrian basin, Spain, Mar. Petrol. Geol., 104358, https://doi.org/10.1016/j.marpetgeo.2020.104358, 2020.

https://doi.org/10.5194/egusphere-2022-1175
Preprint. Discussion started: 18 November 2022

Cámara, P., and Flinch, J.F.: The southern Pyrenees: A salt-based fold-and-thrust belt, in: Permo-Triassic Salt Provinces of Europe, North Africa and the Atlantic Margins, edited by: Soto, J.I., Flinch, J.F., and Tari, G., Elsevier, Amsterdam, Netherland, 395-415, https://doi.org/10.1016/B978-0-12-809417-4.00019-7, 2017.

Carola, E., Tavani, S., Ferrer, O., Granado, P., Quintà, A., Butillé, M., and Muñoz, J.A.: Along-strike extrusion at the transition between thin-and thick-skinned domains in the Pyrenean Orogen (northern Spain), in: Thick-skin-dominated orogens: From initial inversion to full accretion, edited by: Nemčok, M., Mora, A., Cosgrove, J.W. Geol. Soc., London, Spec. Publ., 377(1), 119-140, https://doi.org/10.1144/SP377.3, 2013.

Carola, E., Muñoz, J.A., and Roca, E.: The transition from thick-skinned to thin-skinned tectonics in the Basque-Cantabrian Pyrenees: The Burgalesa Platform and surroundings. Int. J. Earth Sci., 104(8), 2215-2239, https://doi.org/10.1007/s00531-015-1177-z, 2015.

Carrera, N., Muñoz, J.A., Sàbat, F., Mon, R., and Roca, E.: The role of inversion tectonics in the structure of the Cordillera Oriental (NW Argentinean Andes). J. Struct. Geol., 28(11), 1921-1932, https://doi.org/10.1016/j.jsg.2006.07.006, 2006.

Carrera, N. and Muñoz, J.A.: Thick-skinned tectonic style resulting from the inversion of previous structures in the southern Cordillera Oriental (NW Argentine Andes), in: Thick-skin-dominated orogens: From initial inversion to full accretion, edited by: Nemčok, M., Mora, A., Cosgrove, J.W., Geol. Soc., London, Spec. Publ., 377, 77–100, https://doi.org/10.1144/SP377.2, 2013.

Célini, N., Callot, J.-P., Ringenbach, J.-C. and Graham, R.: Jurassic Salt Tectonics in the SW Sub-Alpine Fold-and-Thrust Belt, Tectonics, 39(10), e2020TC006107, https://doi.org/10.1029/2020TC006107, 2020.

Chenin, P., Manatschal, G., Picazo, S., Müntener, O., Karner, G., Johnson, C., and Ulrich, M.: Influence of the architecture of magma-poor hyperextended rifted margins on orogens produced by the closure of narrow versus wide oceans, Geosphere, 13(2), 559-576, https://doi.org/10.1130/GES01363.1, 2017.

Cooper, M.A., Williams, G.D., de Graciansky, P.C., Murphy, R.W., Needham, T., de Paor, D., Stoneley, R., Todd, S.P., Turner, J.P. and Ziegler, P.A.: Inversion tectonics — a discussion, in: Inversion Tectonics, edited by: Copper, M.A., and Williams, G.D., Geol. Soc., London, Spec. Publ., 44, 335-347, https://doi.org/10.1144/GSL.SP.1989.044.01.18, 1989.

Cotton, J., and Koyi, H.: Modelling of thrust fronts above ductile and frictional décollements; examples from The Salt Range and Potwar Plateau, Pakistan. Geol. Soc. Am. Bull., 112(3), 351–363, https://doi.org/10.1130/0016-7606(2000)112<351:MOTFAD>2.0.CO;2, 2000.

Del Ventissette, C., Montanari, D., Bonini, M., and Sani, F.: Basin inversion and fault reactivation in laboratory experiments. J. Struct. Geol., 28, 2067-2083, https://doi.org/10.1016/j.jsg.2006.07.012, 2006.

Dell'Ertole, D., and Schellart, W.P.: The development of sheath folds in viscously stratified materials in simple shear conditions: An analogue approach. J. Struct. Geol., 56, 129-141, https://doi.org/10.1016/j.jsg.2013.09.002, 2013.

Dooley, T.P., and Hudec, M.R.: Extension and inversion of salt-bearing rift systems, Solid Earth, 11, 1187-1204, https://doi.org/10.5194/se-11-1187-2020, 2020.

https://doi.org/10.5194/egusphere-2022-1175
Preprint. Discussion started: 18 November 2022

Dooley, T., McClay, K.R., Hempton, M., and Smit, D.: Salt tectonics above complex basement extensional fault systems: results from analogue modelling, in: Petroleum Geology: North-West Europe and global perspectives – Proceedings of the 6th Petroleum Geology Conference, edited by: Doré, A.G., and Vining, B.A., 6 (1), 1631-1648, Geological Society, London, https://doi.org/10.1144/0061631, 2005.

Espina, R.G.: Extensión mesozoica y acortamiento alpino en el borde occidental de la Cuenca Vasco Cantábrica. Cad. Lab. Xeol. Laxe, 19, 137-150, 1994.

Espina, R.G.: Tectónica extensional en el borde occidental de la Cuenca Vasco- Cantábrica (Cordillera Cantábrica, NO de España). Geogaceta, 20(4), 890 – 892, 1996.

Ferrer, O., McClay, K.R., Sellier, N.C.: Influence of fault geometries and mechanical anisotropies on the growth and inversion of hanging-wall synclinal basins: insights from sandbox models and natural examples, in: The Geometry and Growth of Normal Faults, edited by: Child, C., Holdsworth, R.E., Jackson, C.A.L., Manzocchi, T., Walsh, J.J., Yieldings, G., Geol. Soc., London, Spec. Publ., 439, 487-509, https://doi.org/10.1144/SP439.8, 2016.

Ferrer, O., Carola, E., and McClay, K.: Structural control of inherited salt structures during inversion of domino basement-fault system from an analogue modelling approach. Solid Earth, submitted.

Frasca, G., Manatschal, G., Cadenas, P., Miró, J., and Lescoutre, R.: A kinematic reconstruction of Iberia using intracontinental strike-slip corridors. Terra Nova, 573-581, https://doi.org/10.1111/ter.12549, 2021.

Gallastegui, J.: Estructura cortical de la cordillera y margen continental cantábricos: perfiles ESCI-N, Trabajos de Geología, 22(22), 3-234, https://doi.org/10.17811/tdg.22.2000.3-234, 2000.

García de Cortázar, A., and Pujalte, V.: Litoestratigrafía y facies del Grupo Cabuérniga (Malm-Valanginiense inferior?) al S de Cantabria-NE de Palencia. Cuadernos de Geología Ibérica, 8, 5–21, 1982.

García-Senz, J., Pedrera, A., Ayala, C., Ruiz-Constán, A., Robador, A., and Rodríguez-Fernández, L.R.: Inversion of the north Iberian hyperextended margin: the role of exhumed mantle indentation during continental collision, in: Fold and thrust belts: Structural style, evolution and exploration, edited by: Hammerstein, J.A., Di Cuia, R., Cottam, M.A., Zamora, G., Butler, R.W.H., Geol. Soc., London, Spec. Publ., 490, 177-198, https://doi.org/10.1144/SP490-2019-112, 2019.

Ghani, H., Zeilinger, G., Sobel, E.R., and, Heidarzadeh, G.: Structural variation within the Himalayan fold and thrust belt: A case study from the Kohat-Potwar Fold Thrust Belt of Pakistan. J. Struct. Geol., 116, 34–46, https.//doi.org/10.1016/j.jsg.2018.07.022, 2018.

Gómez, J.J., Goy, A., and Barrón, E.: Events around the Triassic–Jurassic boundary in northern and eastern Spain: a review. Palaeogeogr. Palaeocl., 244(1-4), 89-110, https://doi.org/10.1016/j.palaeo.2006.06.025, 2007.

Granado, P., Ferrer, O., Muñoz, J. A., Thöny, W., and Strauss, P.: Basin inversion in tectonic wedges: Insights from analogue modelling and the Alpine-Carpathian fold-and-thrust belt. Tectonophysics, 703-704(C), 50–68, https://doi.org/10.1016/j.tecto.2017.02.022, 2017.

Granado, P., Roca, E., Strauss, P., Pelz, K., and Munoz, J.A.: Structural styles in fold-and-thrust belts involving early salt structures: The Northern Calcareous Alps (Austria). Geology, 47(1), 51–54, https://doi.org/10.1130/G45281.1, 2018.

https://doi.org/10.5194/egusphere-2022-1175
Preprint. Discussion started: 18 November 2022

Hubbert, M.K.: Mechanical basis for certain familiar geologic structures. Geol. Soc. Am. Bull., 62(4), 355-372, https://doi.org/10.1130/0016-7606(1951)62[355:MBFCFG]2.0.CO;2, 1951.

Iaffa, D.N., Sàbat, F., Bello, D., Ferrer, O., Monn, R., and Gutierrez, A.A.: Tectonic inversion in a segmented foreland basin from extensional to piggy back settings: The Tucumán Basin in NW Argentina. J. S. Am. Earth Sci., 31(4), 457-474, https://doi.org/10.1016/j.jsames.2011.02.009, 2011a.

Iaffa, D.N., Sàbat, F., Muñoz, J.A., Mon, R., and Gutierrez, A.A.: The role of inherited structures in a foreland basin evolution. The Metán Basin in NW Argentina. J. Struct. Geol., 33(12), 1816-1828, https://doi.org/10.1016/j.jsg.2011.09.005, 2011b.

Jackson, M.P., Vendeville, B.C., and Schultz-Ela, D.D.: Structural dynamics of salt systems. Annu. Rev. Earth Pl. Sc., 22(1), 93-117. https://doi.org/10.1146/annurev.ea.22.050194.000521, 1994.

Jaumé, S.C., and Lillie, R.J.: Mechanics of the Salt Range-Potwar Plateau, Pakistan: a fold-and-thrust belt underlain by evaporites, Tectonics, 7(1), 57–71, https://doi.org/ Mechanics of the Salt Range-Potwar Plateau 10.1029/TC007i001p00057, 1988.

Kley, J., Monaldi, C.R., and Salfity, J.A.: Along-strike segmentation of the Andean foreland: causes and consequences, Tectonophysics, 301(1-2), 75-94, https://doi.org/10.1016/S0040-1951(98)90223-2, 1999.

Lagabrielle, Y., Asti, R., Duretz, T., Clerc, C., Fourcade, S., Teixell, A., Labaume, P, Corre, B., and Saspiturry, N.: A review of cretaceous smooth-slopes extensional basins along the Iberia-Eurasia plate boundary: How pre-rift salt controls the modes of continental rifting and mantle exhumation, Earth-Sci. Rev., 201, 103071, https://doi.org/10.1016/j.earscirev.2019.103071, 2020.

Lescoutre, R., and Manatschal, G.: Role of rift-inheritance and segmentation for orogenic evolution: example from the Pyrenean-Cantabrian system, B. Soc. Geol. Fr., 191(1), 18, https://doi.org/10.1051/bsgf/2020021, 2020.

Lescoutre, R., Manatschal, G., and Muñoz, J.A.: Nature, Origin, and Evolution of the Pyrenean-Cantabrian Junction. Tectonics, 40(5), e2020TC006134, https://doi.org/10.1029/2020TC006134, 2021.

López-Gómez, J., Alonso-Azcárate, J., Arche, A., Arribas, J., Barrenechea, J.F., Borruel-Abadía, V., and Díez, J.B.: Permian-Triassic Rifting Stage, in: The Geology of Iberia: A Geodynamic Approach, Volume 5: Active processes: seismicity, active faulting and relief, edited by: Quesada, C., and Oliveira, J.T., 29-112, Springer, Amsterdam, Netherlands, https://doi.org/10.1007/978-3-030-11295-0_3, 2019.

Manatschal, G., Chenin, P., Lescoutre, R., Miró, J., Cadenas, P., Saspiturry, N., Masini, E., Chevrot, S., Ford, M., Jolivet, L., Mouthereau, F., Thinon, I., Issautier, B. and Calassou, S.: The role of inheritance in forming rifts and rifted margins and building collisional orogens: a Biscay-Pyrenean perspective. B. Soc. Geol. Fr., 192 (1), 55, https://doi.org/10.1051/bsgf/2021042, 2021.

Mandl, G., De Jong, L.N.J., and Maltha, A.: Shear zones in granular material. Rock Mech., 9(2-3), 95-144, https://doi.org/10.1007/BF01237876, 1977.

https://doi.org/10.5194/egusphere-2022-1175
Preprint. Discussion started: 18 November 2022

Martínez Catalán, J.R., Arenas, R., García, F.D., Cuadra, P.G., Gómez-Barreiro, J., Abati, J., Castiñeiras, P., Fernández, J., Sánchez, S., Andonaegui, P., González, E., Díez, A., Rubio, F.J., and Valle, B.: Space and time in the tectonic evolution of the northwestern Iberian Massif: Implications for the Variscan belt, in: 4-D Framework of Continental Crust, edited by: Hatcher Jr., R.D., Carlson, M.P.; McBride, J.H., and Martínez-Catalán, J.R., Geol. Soc. Am. Mem., 200, 403–423, https://doi.org/10.1130/2007.1200(21), 2007.

Matte, P.: Accretionary history and crustal evolution of the Variscan belt in Western Europe, Tectonophysics, 196(3–4), 309–337, https://doi.org/10.1016/0040-1951(91)90328-P, 1991.

Mazzoli, S., Basilici, M., Spina, V., Pierantoni, P.P. and Tondi, E.: Space and Time Variability of Detachment- Versus Ramp-Dominated Thrusting: Insights From the Outer Albanides, Tectonics 41(8), e2022TC007274, https://doi.org/10.1029/2022TC007274, 2022.

McClay, K.R.: Analogue models of inversion tectonics, in: Inversion Tectonics, edited by: Cooper, M.A., and Williams, G.D., Geol. Soc., London, Spec. Publ., 44, 41-59, https://doi.org/10.1144/GSL.SP.1989.044.01.04, 1989.

McClay, K.R., and Buchanan, P.G.: Thrust faults in inverted extensional basins, in: Thrust tectonics, edited by: McClay, K.R., 93-104, Springer, Dordrecht, Netherland, https://doi.org/10.1007/978-94-011-3066-0_8, 1992.

McClay, K.R., and White, M.J.: Analogue modelling of orthogonal and oblique rifting, Mar. Petrol. Geol., 12(2), 137-151, https://doi.org/10.1016/0264-8172(95)92835-K, 1995.

Miró, J., Muñoz, J.A., Manatschal, G., and Roca, E.: The Basque–Cantabrian Pyrenees: report of data analysis. B. Soc. Geol. Fr., 191(1), 22, https://doi.org/10.1051/bsgf/2020024, 2020.

Miró, J., Manatschal, G., Cadenas, P., and Muñoz, J.A.: Reactivation of a hyperextended rift system: the Basque-Cantabrian Pyrenees case, Basin Res., 33(6), 3077-3101, https://doi.org/10.1111/bre.12595, 2021.

Molinaro, M., Leturmy, P., Guezou, J.C., Frizon de Lamotte, D., and Eshraghi, S.A.: The structure and kinematics of the southeastern Zagros fold-thrust belt, Iran: From thin-skinned to thick-skinned tectonics, Tectonics, 24(3), TC3007, https://doi.org/10.1029/2004TC001633, 2005.

Muñoz, J.A.: Evolution of a continental collision belt: ECORS-Pyrenees crustal balanced cross-section, in: Thrust tectonics, edited by: McClay, K.R., 235-246, Springer, Dordrecht, Netherland, https://doi.org/10.1007/978-94-011-3066-0_21, 1992.

Muñoz, J.A., Mencos, J., Roca, E., Carrera, N., Gratacós, Ò., Ferrer, O., and Fernández, O.: The structure of the South-Central-Pyrenean fold and thrust belt as constrained by subsurface data, Geol. Acta, 16(4), 439-460, https://doi.org/10.1344/GeologicaActa2018.16.4.7, 2018.

Muñoz, J.A.: Alpine Orogeny: Deformation and Structure in the Northern Iberian Margin (Pyrenees sl), in: The Geology of Iberia: A Geodynamic Approach, Volume 5: Active processes: seismicity, active faulting and relief, edited by: Quesada, C., and Oliveira, J.T., 433-451, Springer, Amsterdam, Netherlands, https://doi.org/ 10.1007/978-3-030-11295-0_9, 2019.

Pedreira, D., Afonso, J.C., Pulgar, J.A., Gallastegui, J., Carballo, A., Fernández, M., García-Castellanos, D., Jiménez-Munt, I., Semprich, J. and García-Moreno, O.: Geophysical-petrological modeling of the lithosphere beneath the Cantabrian

https://doi.org/10.5194/egusphere-2022-1175
Preprint. Discussion started: 18 November 2022

Mountains and the North-Iberian margin: Geodynamic implications. Lithos, 230, 46-68, https://doi.org/10.1016/j.lithos.2015.04.018, 2015.

Pedrera, A., García-Senz, J., Ayala, C., Ruiz-Constán, A., Rodríguez-Fernández, L.R., Robador, A., and González Menéndez, L.: Reconstruction of the exhumed mantle across the North Iberian Margin by crustal-scale 3-D gravity inversion and geological cross section. Tectonics, 36(12), 3155-3177, https://doi.org/10.1002/2017TC004716, 2017.

Pedrera, A., García-Senz, J., Peropadre, C., Robador, A., López-Mir, B., Díaz-Alvarado, J., and Rodríguez-Fernández, L.R.: The Getxo crustal-scale cross-section: Testing tectonic models in the Bay of Biscay-Pyrenean rift system. Earth-Sci. Rev., 212, 103429, https://doi.org/10.1016/j.eartscirev.2020.103429, 2020.

Pinto, L., Muñoz, C., Nalpas, T., and Charrier, R.: Role of sedimentation during basin inversion in analogue modelling, J. Struct. Geol., 32(4), 554-565, https://doi.org/10.1016/j.jsg.2010.03.001, 2010.

Pulgar, J.A., Alonso, J.L., Espina, R.G., and Marín, J.A.: La deformación alpina en el basamento varisco de la Zona Cantábrica, Trabajos De Geología, 21(21), 283–295, https://doi.org/10.17811/tdg.21.1999.283-295, 1999.

Quintana, L., Pulgar, J.A., and Alonso, J.L.: Displacement transfer from borders to interior of a plate: A crustal transect of Iberia, Tectonophysics, 663, 378-398, https://doi.org/10.1016/j.tecto.2015.08.046, 2015.

Quirk, D.G., and Pilcher, R.S.: Flip-flop salt tectonics, in: Salt tectonics, sediments and prospectivity, edited by: Alsop, G.I., Archer, S.G., Hartley, A.J., Grant, N.T., Hodgkinson, R., Geol. Soc., London, Spec. Publ., 363, 245-264. https://doi.org/10.1144/SP363.11, 2012.

Riba, O., Jurado, M.J.: Reflexiones sobre la geologia de la parte occidental de la Depresión del Ebro. Acta Geológica Hispánica, Libro Homenaje a Oriol Riba Arderiu, 27(1/2), 177–193, 1992.

Roca, E., Muñoz, J.A., Ferrer, O., and Ellouz, N.: The role of the Bay of Biscay Mesozoic extensional structure in the configuration of the Pyrenean orogen: Constraints from the MARCONI deep seismic reflection survey, Tectonics, 30(2). https://doi.org/10.1029/2010TC002735, 2011.

Roest, W.R., and Srivastava, S.P.: Kinematics of the plate boundaries between Eurasia, Iberia, and Africa in the North Atlantic from the Late Cretaceous to the present, Geology, 19(6), 613-616, https://doi.org/10.1130/0091-7613(1991)019<0613:KOTPBB>2.3.CO;2, 1991.

Roma, M., Ferrer, O., Roca, E., Pla, O., Escosa, F.O., and Butillé, M.: Formation and inversion of salt-detached ramp-syncline basins. Results from analog modeling and application to the Columbrets Basin (Western Mediterranean), Tectonophysics, 745, 214-228, https://doi.org/10.1016/j.tecto.2018.08.012, 2018a.

Roma, M., Vidal-Royo, O., McClay, K., Ferrer, O., and Muñoz, J.A.: Tectonic inversion of salt-detached ramp-syncline basins as illustrated by analog modeling and kinematic restoration, Interpretation, 6(1), T127-T144, https://doi.org/10.1190/INT-2017-0073.1, 2018b.

Rowan, M.G.: Passive-margin salt basins: Hyperextension, evaporite deposition, and salt tectonics, Basin Res., 26(1), 154-182, https://doi.org/10.1111/bre.12043, 2014.

https://doi.org/10.5194/egusphere-2022-1175
Preprint. Discussion started: 18 November 2022

Rowan, M.G., and Giles, K.A.: Passive versus active salt diapirism, AAPG Bull., 105, 53-63, https://doi.org/10.1306/05212020001, 2020.

Sani, F., Del Ventisette, C., Montanari, D., Bendkik, A., Chenakeb, M.: Structural evolution of the Rides Prerifaines (Morocco): structural and seismic interpretation and analogue modelling experiments, Int. J. Earth Sci. (Geol. Rundsch.), 96, 685-706, htpps://doi.org/10.1007/s00531-006-0118-2, 2007.

Saspiturry, N., Allanic, C., Razin, P., Issautier, B., Baudin, T., Lasseur, E., Serrano, O., and Leleu, S.: Closure of a hyperextended system in an orogenic lithospheric pop-up, Western Pyrenees: The role of mantle buttressing and rift structural inheritance, Terra Nova, 32(4), 253-260, https://doi.org/10.1111/ter.12457, 2020.

Schellart, W.P.: Shear test results for cohesion and friction coefficients for different granular materials: scaling implications for their usage in analogue modelling, Tectonophysics, 324(1-2), 1-16, https://doi.org/10.1016/S0040-1951(00)00111-6, 2000.

Tavani, S., Carola, E., Granado, P., Quintà, A., and Muñoz, J.A.: Transpressive inversion of a Mesozoic extensional forced fold system with an intermediate décollement level in the Basque-Cantabrian Basin (Spain), Tectonics, 32(2), 146-158, https://doi.org/10.1002/tect.20019, 2013.

Tavani, S., Bertok, C., Granado, P., Piana, F., Salas, R., Vigna, B., and Muñoz, J.A.: The Iberia-Eurasia plate boundary east of the Pyrenees, Earth-Sci. Rev., 187, 314-337, https://doi.org/10.1016/j.earscirev.2018.10.008, 2018.

Tozer, R.S.J., Butler, R.W.H., and Corrado, S.: Comparing thin-and thick-skinned thrust tectonic models of the Central Apennines, Italy. *EGU Stephan Mueller Special Publication Series*, 1, 181-194, 2002.

Teixell, A.: Crustal structure and orogenic material budget in the west central Pyrenees, Tectonics, 17(3), 395-406, https://doi.org/10.1029/98TC00561, 1998.

Tugend, J., Manatschal, G., Kusznir, N.J., Masini, E., Mohn, G., and Thinon, I.: Formation and deformation of hyperextended rift systems: Insights from rift domain mapping in the Bay of Biscay-Pyrenees, Tectonics, 33(7), 1239-1276, https://doi.org/10.1002/2014TC003529, 2014.

Tugend, J., Manatschal, G., and Kusznir, N.J.: Spatial and temporal evolution of hyperextended rift systems: Implication for the nature, kinematics, and timing of the Iberian-European plate boundary, Geology, 43(1), 15-18, https://doi.org/10.1130/G36072.1, 2015.

Vendeville, B.C., and Jackson, M.P.: The rise of diapirs during thin-skinned extension, Mar. Petrol. Geol., 9(4), 331-354, https://doi.org/10.1016/0264-8172(92)90047-I, 1992a.

Vendeville, B.C. and Jackson, M.P.A.: The fall of diapirs during thin-skinned extension, Mar. Petrol. Geol., 9 (4), 354-371, https://doi.org/10.1016/0264-8172(92)90048-J, 1992b.

Weijermars, R.: Flow behaviour and physical chemistry of bouncing putties and related polymers in view of tectonic laboratory applications, Tectonophysics, 124(3-4), 325-358, https://doi.org/10.1016/0040-1951(86)90208-8, 1986.

Wilson, Elizabeth P.; Granado, P.; Santolaria, P.; Ferrer, O.; and Muñoz, J.A.: Inversion of transfer zones in salt-bearing systems: Insights from analogue modelling. Solid Earth, submitted.

https://doi.org/10.5194/egusphere-2022-1175
Preprint. Discussion started: 18 November 2022

Withjack, M.O., and Callaway, S.: Active normal faulting beneath a salt layer: an experimental study of deformation patterns in the cover sequence, AAPG Bull., 84(5), 627-651, https://doi.org/10.1306/C9EBCE73-1735-11D7-8645000102C1865D, 2000.

Wu, J.E., McClay, K., Whitehouse, P., and Dooley, T.: 4D analogue modelling of transtensional pull-apart basins, Mar. Petrol. Geol., 26(8), 1608-1623, https://doi.org/10.1016/j.marpetgeo.2008.06.007, 2009.

https://doi.org/10.5194/egusphere-2022-1175
Preprint. Discussion started: 18 November 2022

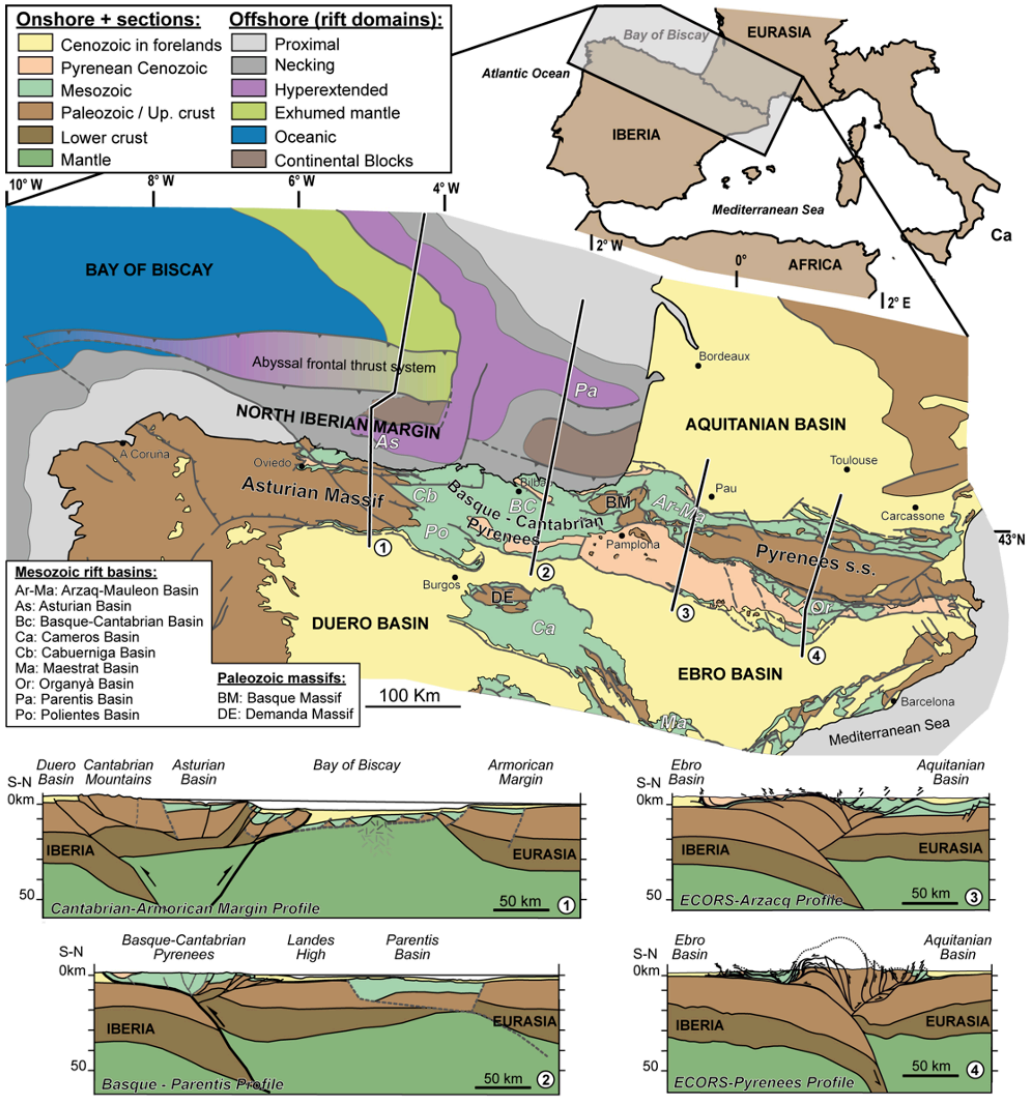

Figure 1: Structural map of the Pyrenean Orogen and surrounding areas with crustal cross-sections depicting the main along-strike structural changes. Rift domains are also mapped offshore. 1) Asturian Massif – Armorican Margin (Cadenas et al., 2018); 2) Basque – Cantabrian Pyrenees – Parentis (Ferrer et al., 2008 and Roca et al. 2011); 3) ECORS-Arzaq (Teixell, 1998); and 4) ECORS-Pyrenees (Muñoz, 1992).

https://doi.org/10.5194/egusphere-2022-1175
Preprint. Discussion started: 18 November 2022

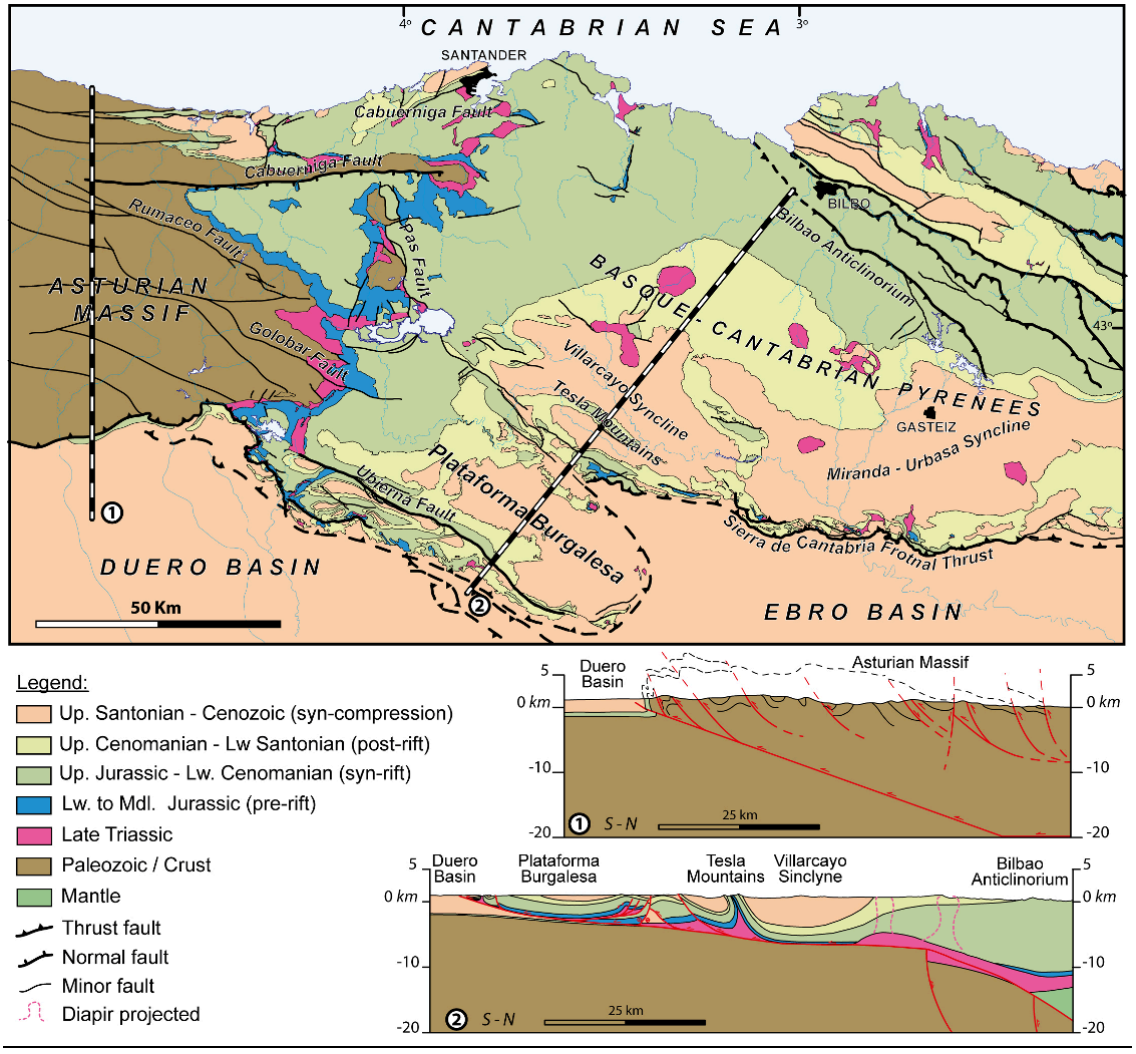

Figure 2: Tectonostratigraphic map of the Basque – Cantabrian Pyrenees – Asturian Massif junction (modified from Miró et al., 2021), and geological cross-section showing the along-strike variability of the structural style, from thick-skinned to the West to thin-skinned to the East. Cross-section 1 from Alonso et al. (1996).

https://doi.org/10.5194/egusphere-2022-1175
Preprint. Discussion started: 18 November 2022

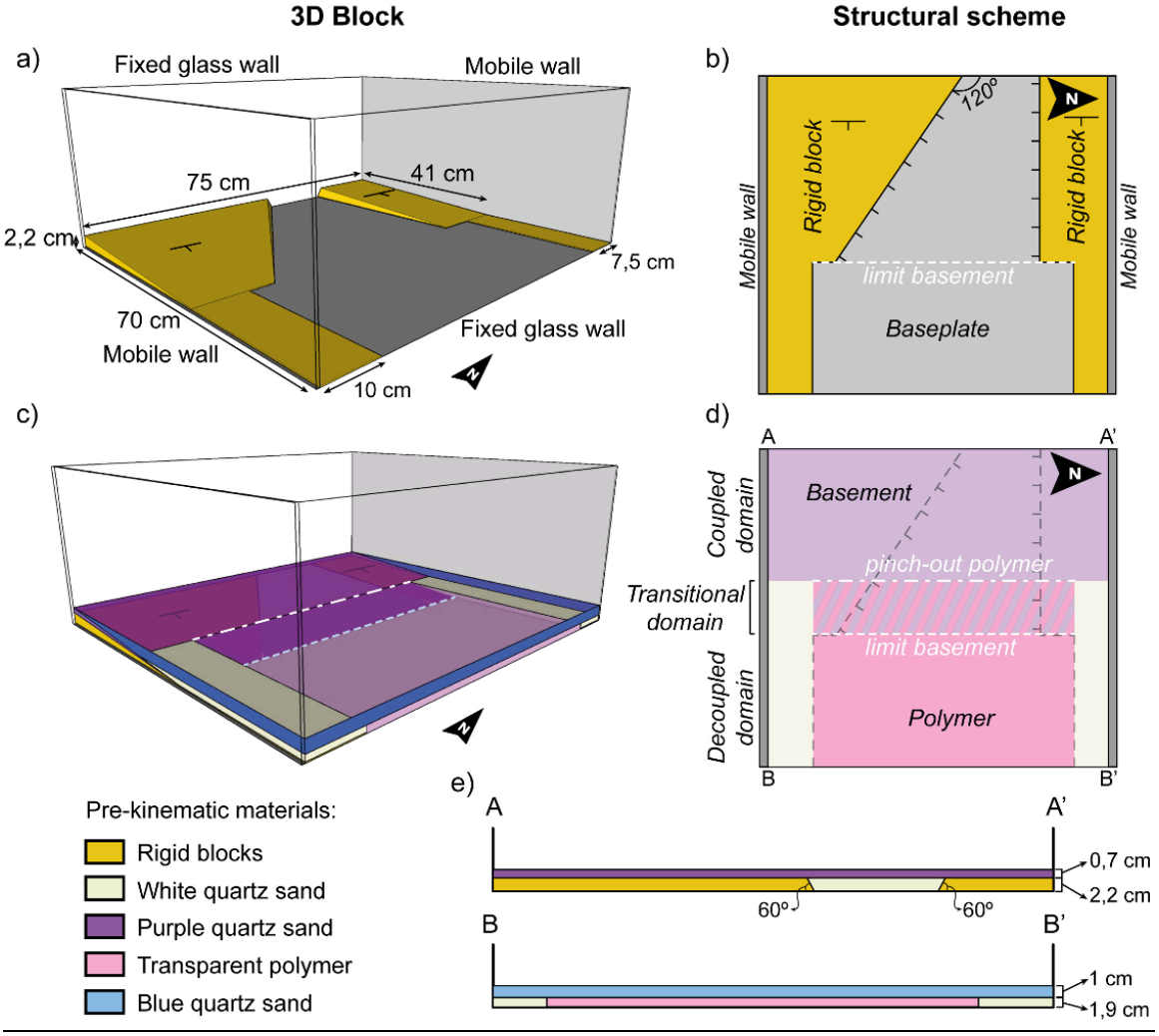

Figure 3: 3D blocks (left) and overhead sketches (right) of the experimental setup. A) 3D block showing the distribution of the rigid blocks at the base of the model. B) Overhead sketch of the previous 3D block. C) Final experimental configuration before extensional deformation showing the distribution of the different layers. The limit of the basement and the pinch out of the polymer are also indicated (see Figure 3D for legend). D) Overhead sketch showing the distribution of basement sand and polymer indicating the overlapping area and the boundaries of both units, which defines the different structural domains. E) Cross-sections of the coupled and decoupled domains prior to extension. See Figure 3D for location.

https://doi.org/10.5194/egusphere-2022-1175
Preprint. Discussion started: 18 November 2022

785

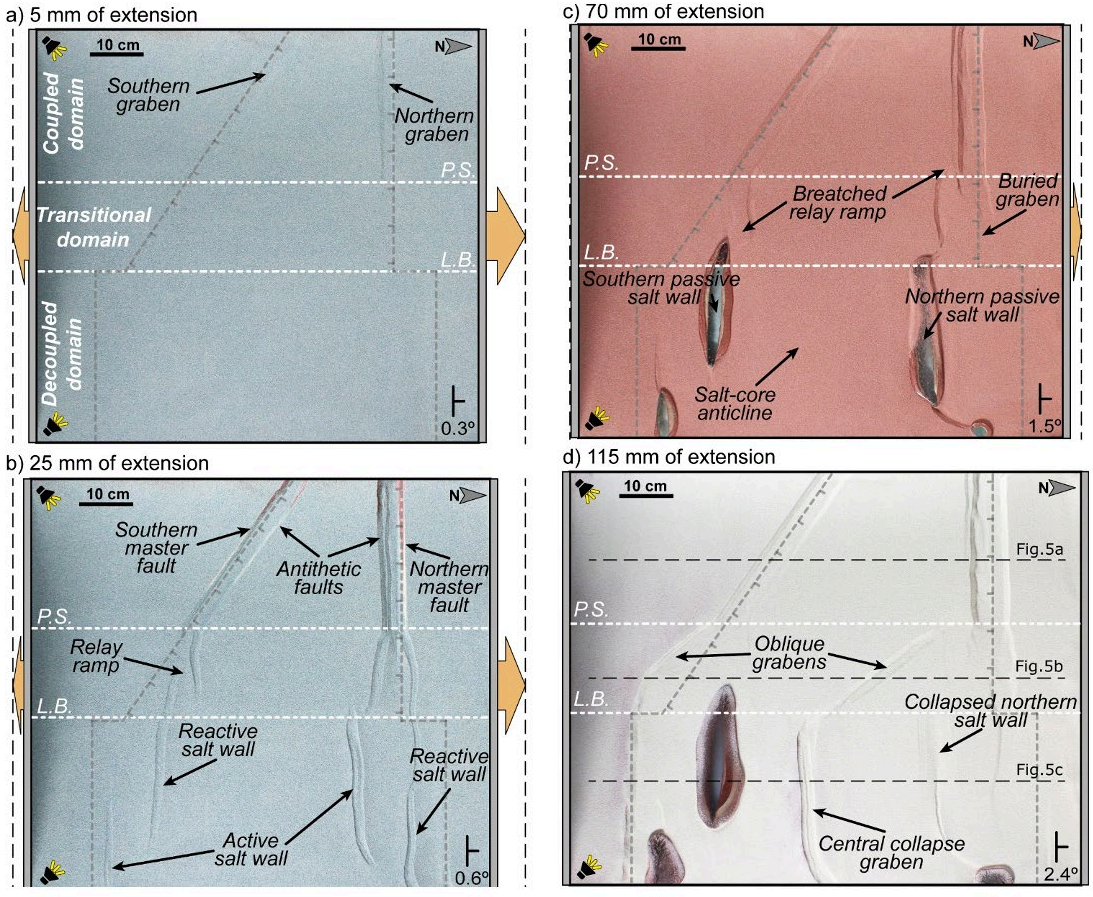

Figure 4: Overhead evolution of Model-1 during extension. Illumination comes from the left. The shadow areas are surface-breaching faults dipping to the right (North) and the illuminated ones are surface-breaching faults dipping to the left (South). The
790 **position of the basement rigid blocks is shown in grey dotted lines, and the polymer pinch out (P.S.) and the limit of basement blocks (L.B.) in white dotted lines. A) Overhead view after 5 mm of extension. B) Overhead view after 25 mm of extension. C) Overhead view after 70 mm of extension. D) Overhead view after 115 mm of extension.**

https://doi.org/10.5194/egusphere-2022-1175
Preprint. Discussion started: 18 November 2022

795

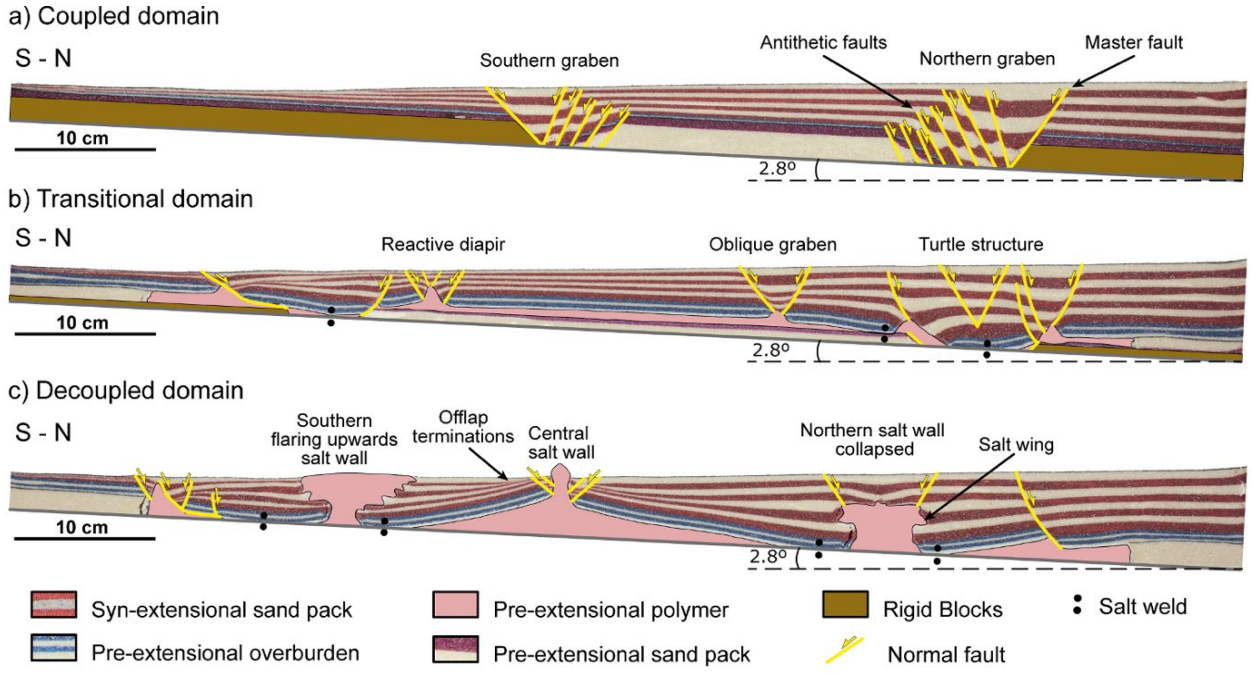

Figure 5: Cross-sections at the end of the extensional deformation (127 mm) across the different structural domains of Model-1. A) Coupled domain; B) Transitional domain; C) Decoupled domain. See Figure 4D for location.

https://doi.org/10.5194/egusphere-2022-1175
Preprint. Discussion started: 18 November 2022

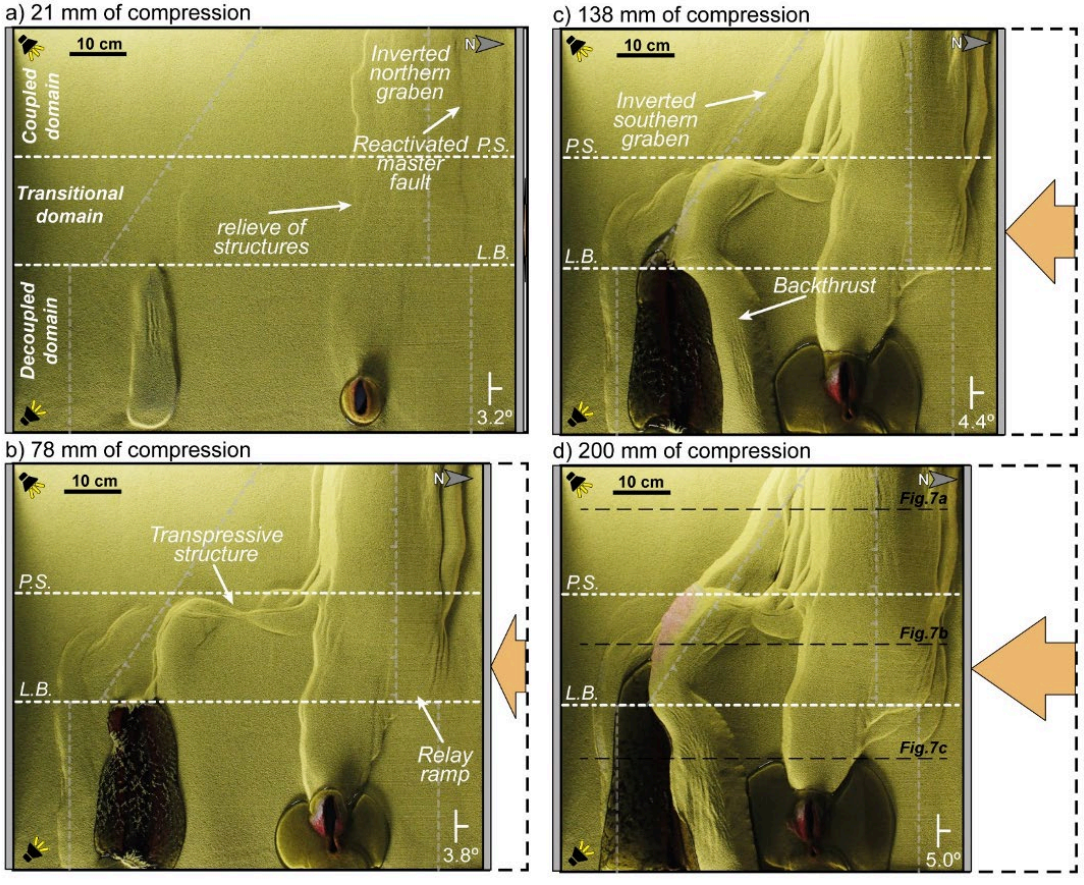

Figure 6: Overhead pictures showing the evolution of Model-2. Illumination comes from the left. The position of the basement rigid blocks is shown in grey dotted lines and the pinch out of the polymer (P.S.) and the limit of basement blocks (L.B.) in white dotted lines. A) Overhead view after 21 mm of shortening. B) Overhead view after 78 mm of shortening. C) Overhead view after 138 mm of shortening. D) Overhead view at the end of the experiment (200 mm shortening).

https://doi.org/10.5194/egusphere-2022-1175
Preprint. Discussion started: 18 November 2022

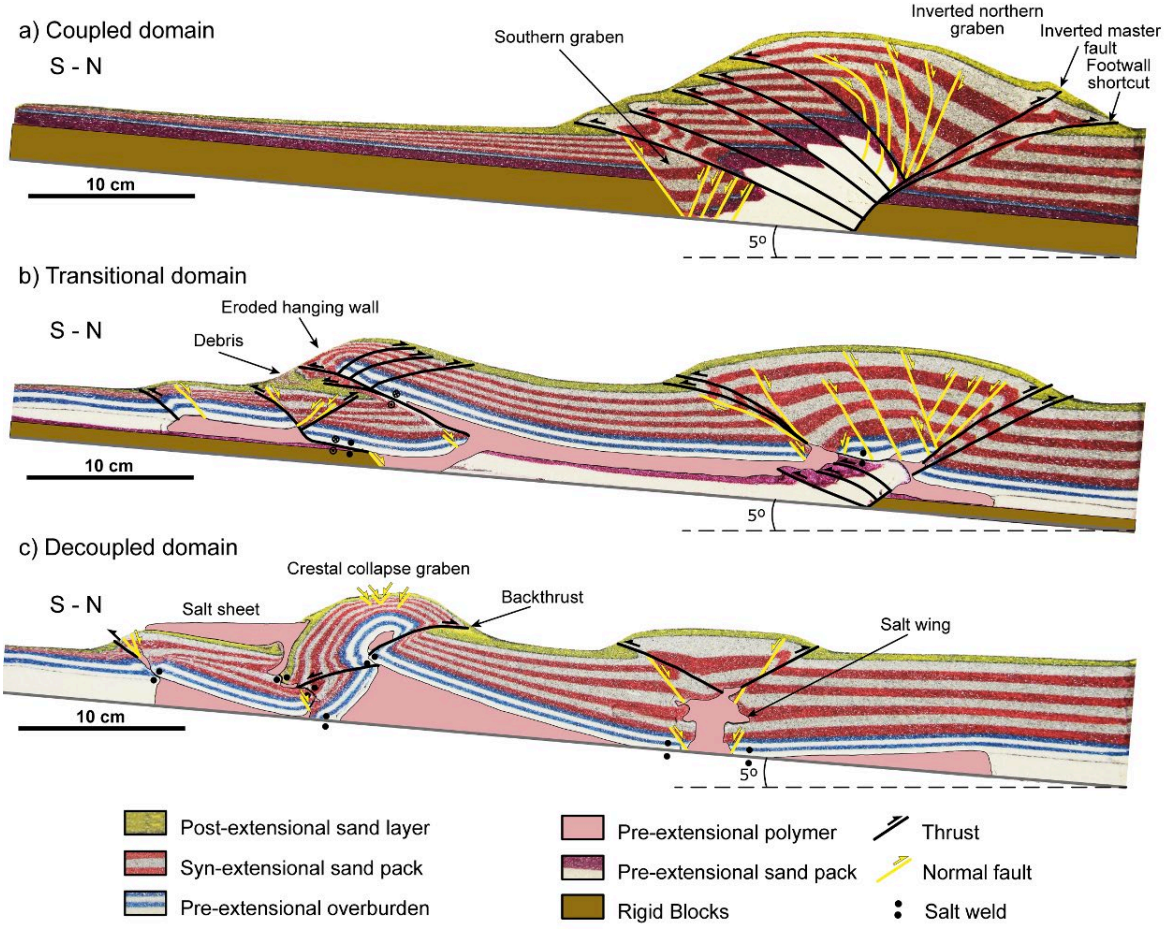

Figure 7: Cross-sections at the end of the Model-2 (after 200 mm of shortening) showing the structural style at the different domains. A) Coupled domain; B) Transitional domain; C) Decoupled domain. See figure 6D for location.

https://doi.org/10.5194/egusphere-2022-1175
Preprint. Discussion started: 18 November 2022

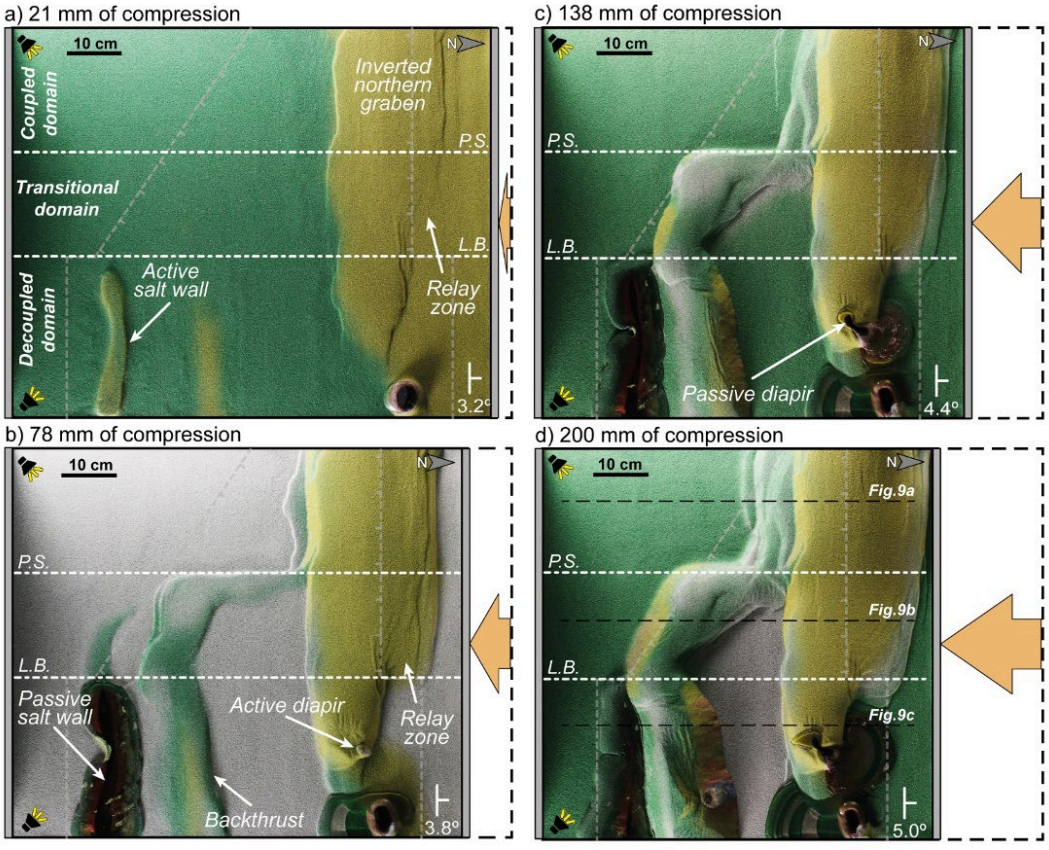

Figure 8: Overhead pictures showing the evolution of Model-3. Illumination comes from the left. The position of the basement rigid blocks is shown in grey dotted lines and the pinch out of the polymer (P.S.) and the limit of basement blocks (L.B.) in white dotted lines. A) Overhead view after 21 mm of shortening. B) Overhead view after 78 mm of shortening. C) Overhead view after 138 mm of shortening. D) Overhead view at the end of the experiment (200 mm shortening).

https://doi.org/10.5194/egusphere-2022-1175
Preprint. Discussion started: 18 November 2022

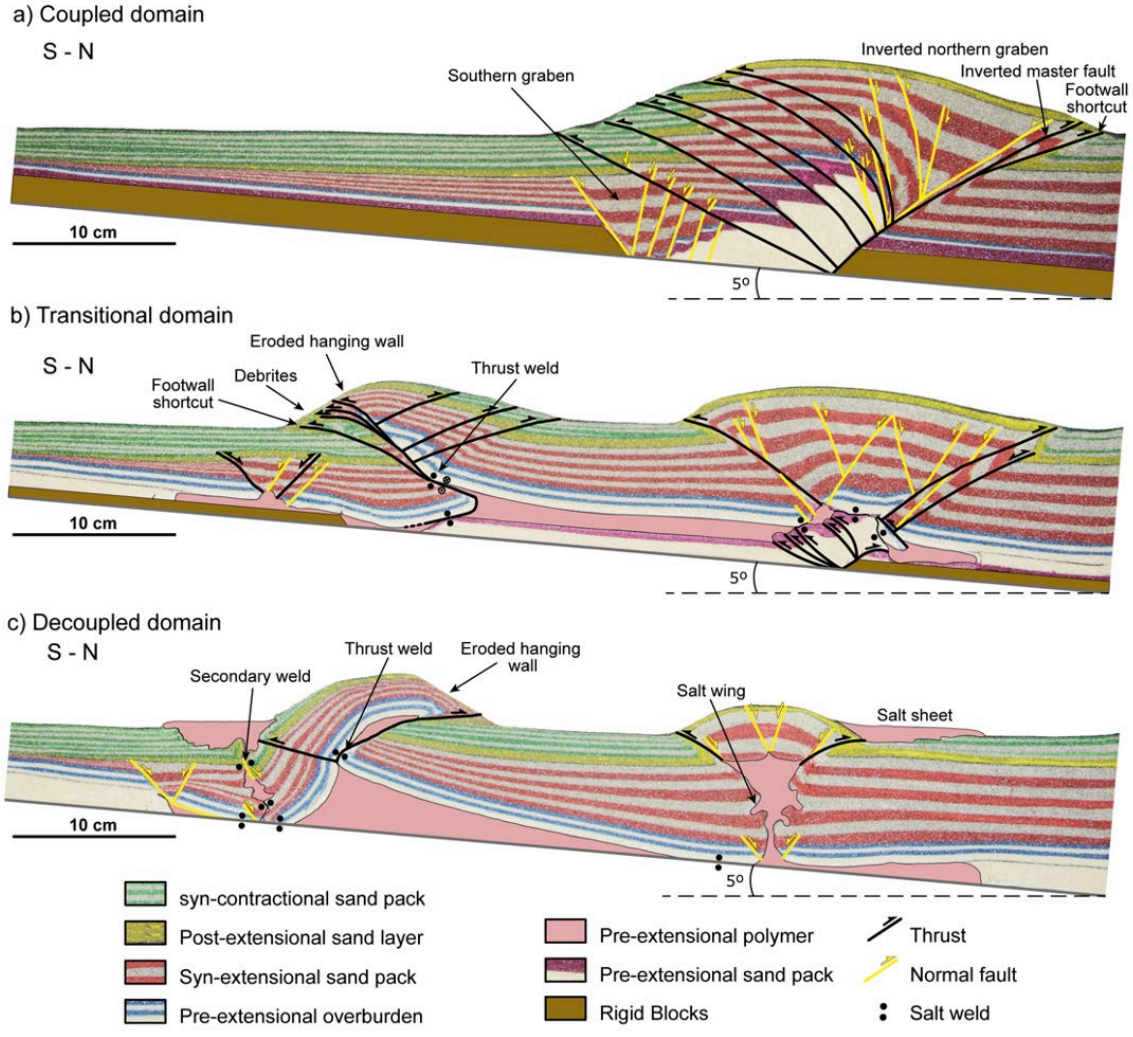

825 **Figure 9: Cross-sections at the end of the Model-3 (after 200 mm of shortening) showing the structural style at the different domains. A) Coupled domain; B) Transitional domain; C) Decoupled domain. See figure 8D for location.**

https://doi.org/10.5194/egusphere-2022-1175
Preprint. Discussion started: 18 November 2022

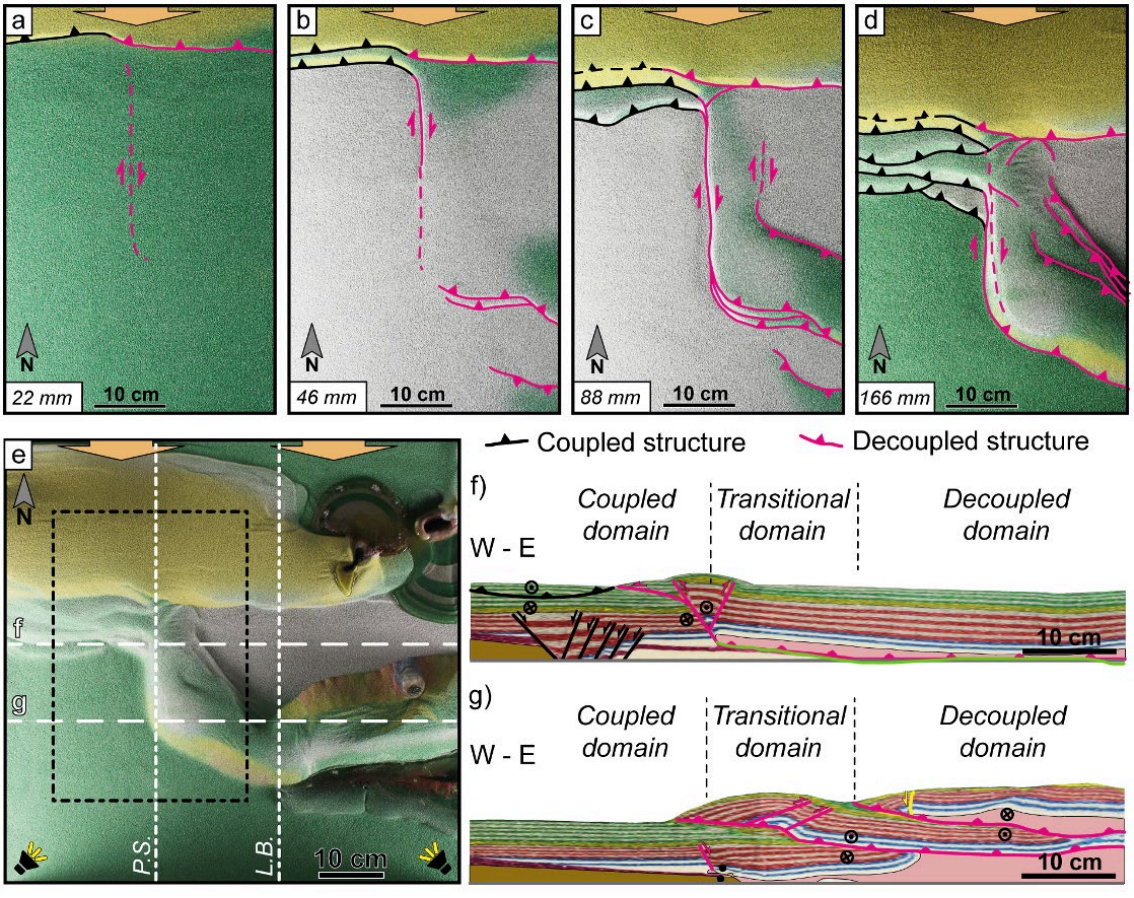

Figure 10: a to d) Detail of the overhead evolution of the transitional domain in Model-3 after 22, 46, 88, and 166 mm of shortening respectively. e) Overhead view at the end of the Model-3 (after 200 mm of shortening). The black square indicates the approximate location of Figure 10d. f and g) W-E cross-sections built from a 3D voxel showing the structural style of the transitional domain (see location in Figure 10e).

https://doi.org/10.5194/egusphere-2022-1175
Preprint. Discussion started: 18 November 2022

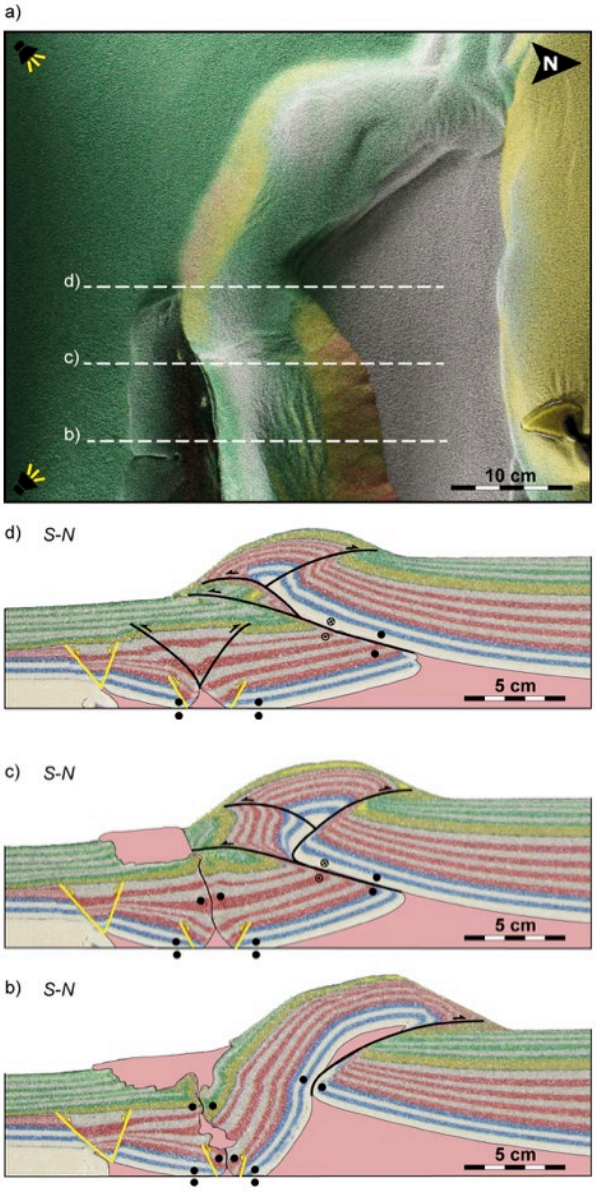

Figure 11: Detailed overhead view of Model-3 at the end of compressional deformation. b) to d) Detailed cross-sections showing the vergence variation between the decoupled and the transitional domains. See section's location in Figure 11a.

https://doi.org/10.5194/egusphere-2022-1175
Preprint. Discussion started: 18 November 2022

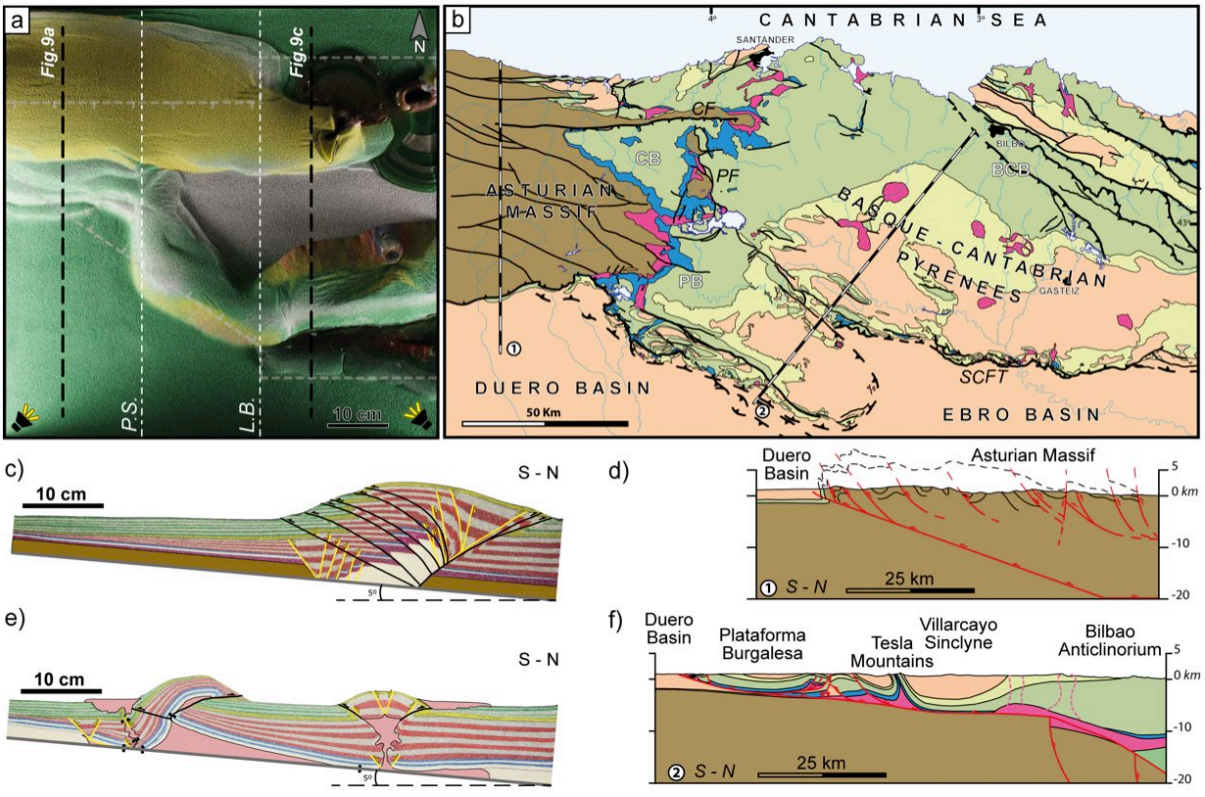

Figure 12: a) Overhead view of Model-3 at the end of the experiment. B) Tectonostratigraphic map of the Basque–Cantabrian Pyrenees – Asturian Massif junction (modified from Miró et al., 2021). C) Cross-section of the coupled domain showing the thick-skinned deformation in Model-3. D) Cross-section through the Asturian Massif (modified from Alonso et al., 1996) showing the thick-skinned deformation similar to what was observed in the model. E) Cross-section through the decoupled domain in Model-3. F) Cross-section across the southern Basque–Cantabrian Pyrenees showing the characteristic thin-skinned deformation of the area.